UNIVERSIDADE DE LISBOA
FACULDADE DE CIÊNCIAS
DEPARTAMENTO DE BIOLOGIA VEGETAL

Developing new molecular tools to study and visualize the intermediate filament GFAP in living cells

Ricardo Jorge Pinheiro Quiteres

Mestrado em Biologia Molecular e Genética

Dissertação orientada por:

Professor Doutor Federico Herrera
Doutor Zach Hensel

2019

Acknowledgments

The completion of this thesis would not have been possible without the help, guidance and support of so, so many people:

I start by thanking my supervisor Dr. Federico Herrera for welcoming me in your group, for your guidance through each stage of this thesis and for all the patience and time you spent teaching me.

I would like to express my deepest gratitude to Dr. Zach Hensel for your tremendous help and advice, even when I was not technically your student.

I am also thankful to Dr. Alvaro Crevenna for all the advice and for the knowledge that he shared.

I also wish to thank the Flow Cytometry and the Advanced Imaging Facilities of Instituto Gulbenkian de Ciência for their services and assistance.

Thank you to all the people from Fede's lab, especially to three very talented PhD students. First to Cristina for all your help with that diabolic technique. To Fernanda thank you for all your help, encouragement and support and for taking time off your experiments to teach me. Finally, to my mentor and friend Ricardo, thank you for your massive help, for teaching me basically everything that I know and for answering an enormous amount of questions and not answering a lot more, allowing me to think and grow as a scientist.

To three of the most kind, helpful and funny people I have ever met. Sara, Soraia and Teresa, thank you so, so much! Through the ups and downs of this thesis, you were always there for me, helping me and giving me advice. I want to specially thank you for the ice creams, for all the lunch hours we spend talking about random stuff and eating stolen chocolates, for getting us lost in the middle of nowhere, for the war games in the lab and for bringing up my goofiest side. Thank you for making this a year I will never forget! Ricciardi forever!

To my family, and especially to my mom, dad, sister and grandparents a massive thank you. Thank you for all your unconditional love and support, for being an inspiration, for always believing in me even when I did not and for always pushing me to do better and to be better. Everything that I accomplished is entirely thanks to you.

Lastly, a special thank you to my grandfather, for everything you taught me and for everything you did for me. Wherever you are I hope you are proud of me.

Abstract

Intermediate filaments (IFs) are one of the three major filaments of the cytoskeleton. Due to their intrinsic physical properties, IFs provide mechanical support and give cells the elastic properties that allow them to resist deformation and maintain their shape. Different from actin filaments and microtubules, IFs have a cell type-specific expression pattern, and in mature astrocytes, the main IF protein expressed is the glial fibrillary acidic protein (GFAP). Although the exact function of GFAP remains unclear, GFAP is overexpressed in response to a variety of insults to the Central Nervous System (CNS) and the deletion of GFAP renders mice more susceptible to neurotoxicity. Furthermore, heterozygous gain-of-function mutations in the *GFAP* gene cause Alexander disease (AxD), a progressive and fatal neurodegenerative disorder that most frequently affects newborns and infants. IFs are the least characterized filaments of the three major cytoskeleton elements. Difficulties in studying the behavior of these filaments, and in particular of GFAP, arise from the fact that these proteins do not tolerate well the presence of protein tags in its termini. Therefore, we aimed to create new and more versatile molecular tools to study the behavior of GFAP in living cells, and that can easily be implemented in the study of other IFs. In this work, we developed a mouse GFAP-HaloTag fused system and the first tagged version of human GFAP. Both versions of tagged GFAP were able to incorporate into the IF network and form a normal filamentous network when transiently transfected in mammalian U251 cells. Opposingly, R236H/R239C AxD-causing mutations disrupted the endogenous filament network of GFAP and altered its diffusion properties. Furthermore, our results also show that GFAP dynamics is intimately linked to that of actin microfilaments and microtubules, as cytoskeleton-destabilizing drugs completely change the diffusion properties of GFAP molecules. Taken together, the results in this thesis demonstrate the enormous potential our two novel systems have for the study of GFAP oligomerization, aggregation, and dynamics in living cells.

Keywords: Astrocytes, Intermediate filaments, GFAP, Alexander disease, HaloTag

Resumo

A habilidade de uma célula de resistir a deformação, transportar carga intracelular ou de mudar a sua forma durante o movimento depende do citoesqueleto. O citoesqueleto é uma rede complexa de filamentos proteicos e proteínas motoras associadas que se estende pelo citoplasma de todas as células, incluindo bactérias e arquea. Em células eucarióticas, o citoesqueleto é composto por três tipos de polímeros, distinguíveis entre si pelo tamanho: filamentos de actina ou microfilamentos (7 nm de diâmetro), microtúbulos (24 nm) e filamentos intermédios (10 nm). Contrariamente aos microfilamentos e microtúbulos, cuja composição é muito semelhante entre todos os tipos celulares, a composição dos filamentos intermédios varia consideravelmente entre diferentes tipos de células, tecidos e órgãos, durante o desenvolvimento e em condições patológicas. Os filamentos intermédios são estruturas extremamente estáveis que fornecem suporte e protegem as células de danos mecânicos ao conferir-lhes propriedades elásticas para resistir à deformação e manter a sua forma. Além destas funções de suporte, estes filamentos desempenham ainda um papel na sobrevivência, divisão e migração celular. Devido à multitude de funções nas quais os filamentos intermédios participam, alterações nos níveis de expressão ou mutações em componentes específicos destes filamentos estão associadas ao aparecimento de várias patologias, a sua grande maioria raras. Apesar da sua enorme estabilidade, os filamentos intermédios são estruturas bastante dinâmicas e muitas vezes a participação dos microtúbulos e dos filamentos de actina é fundamental para a manutenção da sua rede.

A proteína ácida fibrilar glial (GFAP) é o filamento intermédio mais característico dos astrócitos, e é universalmente utilizada como o principal marcador para a sua identificação e classificação. Apesar da estrutura tridimensional desta proteína permanecer desconhecida, pensa-se que possua uma estrutura tripartida que é semelhante entre todos os filamentos intermédios. Esta estrutura consiste num domínio central alfa-helicoidal altamente conservado flanqueado por dois domínios N-terminal e C-terminal, sem uma estrutura secundária definida. Assim como os restantes filamentos intermédios, a GFAP tende a formar filamentos com 10 nm de diâmetro. Primeiramente, ocorre a formação de um dímero através da interação entre os domínios centrais de dois monómeros, que se enrolam um sobre o outro para formar uma estrutura superenrolada. De seguida, estes dímeros associam-se de forma antiparalela para formar tetrâmeros apolares. Posteriormente, com a contribuição dos domínios N-terminais, os tetrâmeros associam-se para formar protofilamentos que, por sua vez, se associam lateralmente para formar os filamentos maturos, com vários nanómetros de comprimento. Contrariamente aos restantes filamentos do citoesqueleto, a construção dos filamentos intermédios é totalmente independente de nucleótidos. Para além de fornecer suporte mecânico aos astrócitos, pensa-se que a GFAP tenha também um papel importante na migração e motilidade celular, na mitose e ainda na manutenção da barreira hematoencefálica. A GFAP está também associada a várias patologias do sistema nervoso central, tais como a doença de Alexander. A doença de Alexander é uma doença neurodegenerativa rara, fatal e progressiva que afeta essencialmente recém-nascidos e crianças. Esta doença resulta do aparecimento de mutações pontuais no gene que codifica para a GFAP e é caracterizada pela acumulação massiva deste filamento intermédio, juntamente com proteínas de stress, em estruturas citoplasmáticas complexas, denominadas por fibras de Rosenthal.

Atualmente, os filamentos intermédios são os polímeros menos caracterizados do citoesqueleto e o nosso conhecimento atual relativamente à sua estrutura tridimensional, bem como dos processos dinâmicos envolvidos na sua construção, está muito longe de estar completo. Esta escassez de conhecimento relativamente à organização e dinâmica dos filamentos intermédios deve-se em parte à dificuldade em visualizar estes filamentos *in vivo*. Isto acontece porque estes filamentos, e em particular a GFAP, não toleram bem a presença de marcadores proteicos nos seus terminais, como por exemplo as proteínas

fluorescentes, já que estes causam a rutura ou desorganização dos filamentos e levam à sua agregação. Assim, o principal objetivo deste trabalho é desenvolver novos modelos celulares para o estudo da oligomerização, função e dinâmica da GFAP em células vivas.

No presente estudo, começámos por construir um plasmídeo no qual a GFAP de ratinho foi ligada a uma HaloTag (mGFAP-HT), de forma a puder estudar a arquitetura e o comportamento da GFAP a um nível nanoscópico. A HaloTag é uma alternativa atrativa às proteínas fluorescentes, uma vez que combina a especificidade genética destas proteínas com as propriedades foto-físicas superiores de ligandos orgânicos, uma característica que a torna muito apelativa para microscopia de super-resolução e outras técnicas avançadas. Neste trabalho desenvolvemos também com sucesso a primeira versão marcada da GFAP de humano inserindo, de forma aleatória, a proteína fluorescente EGFP dentro da região codificante da GFAP. Quando expressos transientemente nas células de glioblastoma humano U251, ambos os sistemas foram capazes de se integrar na rede de filamentos intermédios endógena destas células e de formar estruturas filamentosas típicas da GFAP em aproximadamente 90% das células.

Por forma a estudar o efeito que as mutações relacionadas com a doença de Alexander têm na construção dos filamentos da GFAP, gerámos o mutante de ratinho R236H e o mutante de humano R239C, por mutagénese dirigida. Os nossos resultados mostram que na maioria das células transfetadas com os plasmídeos mutantes, a GFAP não é capaz de formar uma rede filamentosa. No entanto, o comportamento da GFAP mutante não é o mesmo nos dois modelos. Enquanto que o mutante de humano R239C formou maioritariamente pequenos agregados, o mutante de ratinho R236H formou um padrão homogéneo disperso pelo citoplasma das células, sem nenhuma estrutura filamentosa aparente. Embora vários esforços continuem a ser feitos para tentar encontrar um composto que seja eficaz contra a doença de Alexander, a verdade é que esta doença permanece intratável e incurável. No entanto, estudos recentes demonstraram que a especiaria curcumina tem um efeito benéfico na redução da agregação da GFAP. Desta forma, decidimos testar o efeito neuroprotetor de dois compostos sintéticos e derivados da curcumina, J147 e CNB-001, na redução da agregação do mutante humano R239C. Observámos que, no nosso modelo celular, o composto CNB-001 é mais eficaz que o J147 e que apenas as células que cresceram na presença de CNB-001(10 μM) mostraram um aumento ligeiro, embora significativo, na formação de filamentos e uma respetiva diminuição da agregação da GFAP.

O plasmídeo mGFAP-HT foi ainda utilizado para estudar a dinâmica da GFAP de ratinho. Os nossos resultados mostram que a mutação R236H tem um forte efeito na dinâmica da GFAP, aumentando consideravelmente a sua velocidade de difusão, comparativamente à GFAP não mutada. Os filamentos intermédios estão em constante comunicação com os restantes elementos do citoesqueleto, e muitas vezes a sua dinâmica está dependente destes. Os nossos resultados são consistentes com estas observações, e demonstram que a despolimerização dos microfilamentos de actina ou dos microtúbulos resulta numa diminuição significativa da velocidade de difusão das moléculas de GFAP, e num aumento da percentagem de moléculas com uma difusão mais lenta.

Em suma, os resultados apresentados neste trabalho demonstram o enorme potencial dos dois sistemas que construímos no estudo da função, oligomerização e dinâmica da GFAP em células vivas. Em teoria, estas estratégias, podem também ser utilizadas para o estudo de qualquer outro filamento intermédio. O desenvolvimento de novos e mais versáteis modelos celulares, continua, no entanto, a ser indispensáveis para uma melhor compreensão do comportamento da GFAP em células vivas e também dos mecanismos pelos quais mutações nesta proteína causam a doença de Alexander.

Palavras-chave: Astrócitos, Filamentos intermédios, GFAP, Doença de Alexander, HaloTag

General Contents

Index of Figures

Index of Tables

List of Abbreviations

Aa	Amino acids
Amp	Ampicillin
AxD	Alexander Disease
BiFC	Biomolecular Fluorescence Complementation
bp	Base Pairs
BSA	Bovine Serum Albumin
Ca^{2+}	Calcium Ion
cm	Centimeter
CNS	Central Nervous System
CNTF	Ciliary Neurotrophic Factor
CO_2	Carbon Dioxide
CON	Control
DMEM	Dulbecco's Modified Eagle Medium
DMSO	Dimethyl Sulfoxide
DNA	Deoxyribonucleic Acid
dNTPs	Deoxynucleotides
E. coli	*Escherichia coli*
EGFP	Enhanced Green Fluorescent Protein
EM	Electron-Multiplying
EM-CCD	Electron-Multiplying Charge-Coupled Device
ER	Endoplasmic Reticulum
FBS	Fetal Bovine Serum
GAPDH	Glyceraldehyde-3-Phosphate Dehydrogenase
GFAP	Glial Fibrillary Acidic Protein
GFP	Green Fluorescent Protein
GLT-1	Glutamate Transporter 1
h	Hour
hGFAP	Human Glial Fibrillary Acidic Protein
HRP	Horseradish Peroxidase
HT	HaloTag
IFs	Intermediate Filaments
IgG	Immunoglobulin G
IL-6	Interleukin-6
JAK	Janus Kinase
JF549	Janelia Fluor 549 nm
JF646	Janelia Fluor 646 nm
JNK	c-Jun N-terminal Kinase
kan	Kanamycin
kb	Kilobase
kDa	Kilodalton
kW	Kilowatt
LB	Luria Broth
LIF	Leukemia Inhibitory Factor
MAPK	Mitogen-Activated Protein Kinase
Mg^{2+}	Magnesium Ion
mGFAP	Mouse Glial Fibrillary Acidic Protein

MHz	Megahertz
min	Minute
ml	Milliliter
mM	Millimolar
mRNA	Messenger RNA
ms	Millisecond
mTOR	Mammalian Target of Rapamycin
mW	Milliwatt
NaAz	Sodium Azide
NaCl	Sodium Chloride
NF-kB	Nuclear Factor kappa-light-chain-enhancer of activated B cell
ng	Nanogram
nm	Nanometer
nM	Nanomolar
Nrf2	Nuclear Factor Erythroid 2-Related Factor 2
p	p-Value
PA-JF549	Photoactivatable Janelia Fluor 549 nm
PBS	Phosphate Buffer Saline
PCR	Polymerase Chain Reaction
PNS	Peripheral Nervous System
RFs	Rosenthal Fibers
sCMOS	Scientific Complementary Metal-Oxide-Semiconductor
SD	Standard Deviation
SDS	Sodium Dodecyl Sulphate
SDS-PAGE	Sodium Dodecyl Sulphate - Polyacrylamide Gel Electrophoresis
s	Second
SRRF	Super-Resolution Radial Fluctuations
STAT3	Signal Transducer of Activators of Transcription
TAE	Tris-Acetate-EDTA
TBS	Tris-HCl Buffer Saline
TBST	Tris-HCl Buffer Saline-Tween 20
ULFs	Unit Length Filaments
UTR	Untranslated Region
V	Volt
V1	Venus 1
V2	Venus 2
WT	Wild-Type
µg	Microgram
µl	Microliter
µm	Micrometer
µM	Micromolar

1. Introduction

1.1. Intermediate Filaments: a key component of the cytoskeleton

The structural framework of a cell is provided by the cytoskeleton, a complex network of proteinaceous filaments and motor proteins that extends throughout the cytoplasm of all cells, including bacteria and archaea[1]. The cytoskeleton is an adaptive and dynamic structure that helps cells divide, move, maintain their shape and regulate the traffic of intracellular cargo through the cytoplasm, among other important functions[2]. Three major types of polymers, distinguishable by their size, make up the cytoskeleton of eukaryotic cells: actin filaments or microfilaments, microtubules, and a group of polymers collectively known as intermediate filaments (IFs). Microtubules are formed by a few isoforms of tubulin and are the thickest filaments with a typical diameter of 24 nm. These filaments are constantly assembling and disassembling and play a crucial role in cell division and migration, and in the transport of intracellular cargo. Microfilaments are mainly formed by actin isoforms and reach 7 nm in diameter. They are involved in a variety of processes that require force, including muscle contraction and cell exploration and movement. Lastly, intermediate filaments, as the name suggests, have a diameter that falls between that of actin microfilaments and microtubules. These 10 nm-diameter filaments provide support for microfilaments and microtubules and give cells elastic properties that allow them to withstand tension[1-4].

In contrast to actin filaments and microtubules, the composition of the proteins making up intermediate filaments varies considerably between different tissues, organs, and cell types, during development or in pathological conditions[5]. Intermediate filaments are classified into five major types based on similarities in amino acid sequence, protein structure predictions, and assembly properties[6]. Because IFs play such an important role in providing mechanical support to cells, changes in expression levels or mutations of specific IF components are associated with a multitude of tissue-specific degenerative disorders[7,8] (**Table 1.1**).

Table 1.1: Classification of Intermediate filaments and associated pathologies.

Class	Proteins	Localization	Examples of diseases
I and II	Acidic and neutral-basic keratins	Epithelial cells	Epidermolysis bullosa simplex; epidermolytic hyperkeratosis; monilethrix; keratodermas;
III	Vimentin	Mesenchymal cells	Dominant cataracts
	GFAP	Astrocytes	Alexander disease
	Desmin	Muscle	Desmin-related myopathy
	Peripherin	Peripheral neurons	Amyotrophic lateral sclerosis 1
	Syncoilin	Muscle	Desminopathy; muscular dystrophy
IV	Neurofilaments	Central Nervous System	Various Charcot-Marie-Tooth diseases; Parkinson disease
	a-Internexin	Central Nervous System	Amyotrophic lateral sclerosis; dementia
	Nestin	Glial and neural precursor cells	-
	Synemin	Muscle	Various cancers
V	Lamins (A, B1, B2, C)	Cell nucleus	Hutchinson-Gilford progeria syndrome; Acquired partial lipodystrophy
Orphans (VI)	Bfsp1 (filensin) Bfsp2 (phakinin)	Lens cells	Autosomal-dominant cataract Autosomal-recessive cataract

All IFs share a common tripartite structure consisting of a highly conserved α-helical central domain (rod domain) flanked by an amino (N)-terminal head domain and a carboxy (C)-terminal tail domain (**Figure 1.1**). The rod domain is divided into four hydrophobic α-helical segments of conserved length: 1A, 1B, 2A and 2B. These four segments are interconnected by three short linkers (L1, L12, and L2). The beginning and end parts of the rod domain are particularly conserved in all IFs. Both of these conserved regions are involved in dimer-dimer interactions and mutations in these regions are deleterious to IF organization and dynamics. On the contrary, the head and tail domains have very little secondary structure and their length and sequence vary considerably among different IF proteins.[9-11] The three-dimensional structures of most IFs, including GFAP, remain incompletely described and this is a major barrier to our understanding of their assembly, protein-protein interactions, and other functional properties.

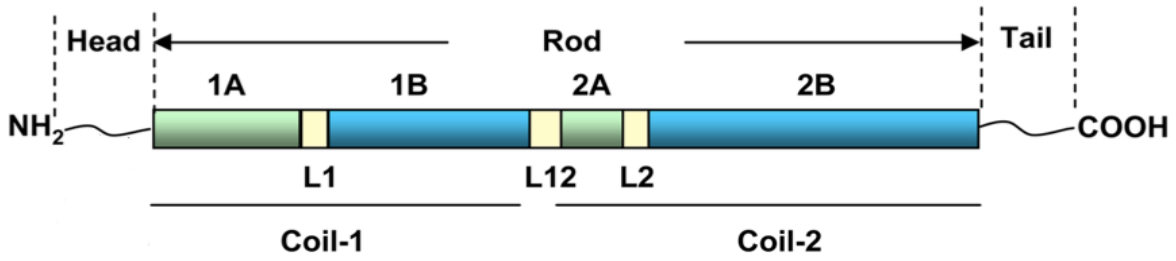

Figure 1.1: Schematic representation of IF protein structure. All IFs share a common tripartite structure with a conserved central rod domain flanked by a N-terminal head domain and a C-terminal tail domain.

Intermediate filaments are very stable structures and until recently they were thought to have very limited dynamics when compared to actin filaments and microtubules. This assumption originated from the observation that most IFs in a cell were not extracted and remained intact after cell lysis with detergents and high concentrations of salts[12]. However, recent studies demonstrated that IFs are highly dynamic structures that can shorten, elongate and rearrange in response to a wide variety of extracellular or intracellular stimuli[13]. IF dynamics often requires the participation of microtubules and actin filaments. This contribution is particularly important in astrocytes, where microtubule- and actin-dependent transport are essential for the maintenance of the IF network[14].

Besides providing mechanical support to cells, IFs can also interact with cellular organelles either by forming cage-like structures around the nucleus, physically controlling their shape, position, and movement[15,16]; or by serving as anchoring structures for mitochondria, positioning them near high-energy-demanding sites[17]. Furthermore, a large body of evidence points to a key role for IFs in cell survival[18], division[19,20] and migration[21,22].

1.2. Glial Fibrillary Acidic Protein (GFAP) is a major intermediate filament typical of astrocytes

Astrocytes are the most numerous cells in the human brain, outnumbering neurons by over fivefold. These specialized glial cells that display an enormous heterogeneity in their morphology and function were originally thought to have only a passive role in the central nervous system (CNS) in the maintenance of neurons. However, over the past few decades, it has become clear that glial cells, particularly astrocytes, are involved in a wider variety of functions, vital for brain development, physiology and pathology[23]. The most characteristic IF protein expressed in astrocytes is the glial fibrillary acidic protein (GFAP), being universally used as a molecular marker for their identification and classification. This protein was initially discovered and isolated from patients with multiple sclerosis[24] and its amino acid composition was presented for the first time in 1969[25]. GFAP, together with vimentin and nestin,

makes up the intermediate filament system of astrocytes[26]. As astrocytes mature, typically GFAP expression increases, the nestin expression stops and vimentin expression decreases[27,28]. However, not all populations of astrocytes express GFAP and different combinations of IF expression profiles are possible[29].

The human GFAP gene is located on chromosome 17q21 and has nine exons and eight introns distributed over 10 kb in the human genome[30]. There are at least nine GFAP isoforms resulting from alternative mRNA splicing[31,32] (**Figure 1.2**). In humans, GFAP-α is the predominant isoform in the CNS. It has 432 amino acids and a molecular weight of 50 kDa. GFAP-β is highly expressed in non-myelinating Schwann cells in the peripheral nervous system (PNS) and has an alternative upstream transcriptional start site in the 5' UTR. The GFAP-δ isoform is the second most studied isoform and is differentially expressed in neurogenic astrocytes in the subventricular zone and the olfactory bulb. This isoform has 431 amino acids and is generated by alternative mRNA splicing combined with alternative polyadenylation of the intron 7, which generates a new exon E7a. Due to differences in the tail region, this isoform is no longer capable of assembling homomeric GFAP-δ filaments but can form heteromeric intermediate filaments with GFAP-α or vimentin. Other isoforms include the GFAP-γ isoform which lacks exon 1 and includes the last 126 nucleotides of intron 1-2; the splice variants GFAPΔEx6, GFAPΔ164 and GFAPΔ135 that skip sequences in exon 6; the GFAP-κ isoform that lacks exons 8 and 9 like GFAP-δ but the exon 7a is replaced by exon 7b, with the entire intron 7; and the GFAP-ζ isoform, a transcript that includes the last 284 nucleotides of intron 8. The amino acid sequence of human GFAP-α has a very high similarity (91% identity and 95% positivity) to that of mouse GFAP (430 amino acids)[33].

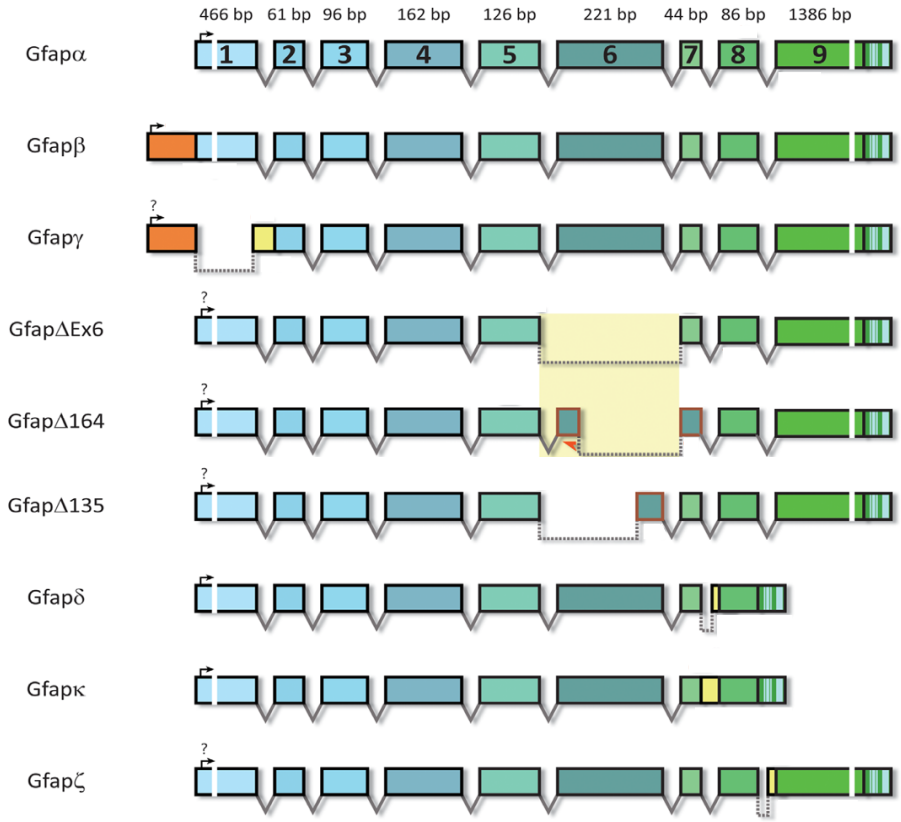

Figure 1.2: Different GFAP isoforms. At least nine GFAP transcript isoforms resulting from alternative mRNA splicing can be found in the central and peripheral nervous systems. Adapted from [32].

Although the three-dimensional structure is unknown, it is believed that GFAP shares with other intermediate filaments a common structure with three major domains: a head domain with 72 amino acids (1-72 Aa), a central helical rod domain with 305 amino acids (73-377 Aa) and a (C)-terminal tail domain with 55 amino acids (378-432 Aa)[34]. Like other intermediate filament proteins, GFAP forms 10 nm diameter filaments. The first stage of filament assembly is the formation of a dimer through the interaction of the rod domain of two polypeptide chains that wind around each other in a coiled-coil structure. These dimers then associate in an anti-parallel manner to form apolar tetramers, which are the initial building blocks of all IFs. With the contribution of the nonhelical tail domains, these tetramers then associate to form protofilaments, and eight protofilaments wind around each other to form unit-length filaments (ULFs) that are 20 nm in diameter. Finally, the ULFs associate longitudinally to form filaments with hundreds of nanometers in length[11,35]. The extended filaments undergo radial compaction that reduces the diameter to 10 nm (**Figure 1.3**)[36]. Unlike microfilaments and microtubules, the assembly of GFAP is totally nucleotide-independent [35].

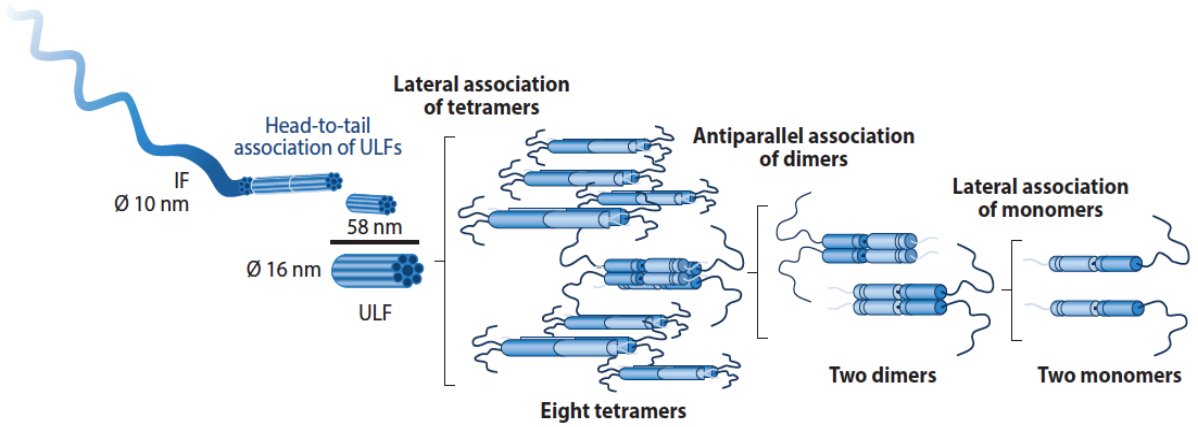

Figure 1.3: Representative scheme of IFs assembly. In the first stage of filament assembly, two GFAP molecules interact to form dimers. Two dimers associate in an anti-parallel manner to form apolar tetramers. Mature IFs are formed by the longitudinal association of unit length filaments (ULFs), that result from the association of apolar tetramers. Adapted from [35].

IFs are often subject to multiple post-translational modifications and GFAP is no exception. Phosphorylation, for example, plays a major role in the regulation of filament assembly/disassembly and in the structural organization of GFAP and other IFs[37-39]. Site-specific phosphorylation of GFAP by protein kinase A, calmodulin-dependent protein kinase II or protein kinase C is responsible for the disassembly of the filaments. The majority of phosphorylation sites are located in the head domain. Of the six phosphorylation sites identified, five (Thr-7, Ser-8, Ser-13, Ser-17, and Ser-34) occur in the head domain; the remaining one, Ser-389, is located in the tail domain[38,39]. Most of the amino acids that are subject to phosphorylation in the head domain of GFAP are conserved among species and GFAP isoforms, which reinforces the physiological importance of phosphorylation in the regulation of GFAP fibrillization[31]. GFAP can also be citrullinated in its arginine residues, which creates epitopes that evoke autoimmune responses[40]. Importantly, studies on post-translational modification were carried out in cell-free, *in vitro* systems using protein extracts or in fixed cells. This limitation was due, in part, to the lack of chimeric versions of GFAP that allowed their visualization in living cells until very recently[14]. IFs including GFAP, rarely tolerate protein tags directly fused to their N- or C-termini, and this constitutes a major hurdle in our understanding of the physio- and pathological functions of this protein.

Similar to other IFs, GFAP is thought to provide mechanical support to astrocytes and help these cells to maintain their mechanical strength as well as their shape. However, the exact functions of GFAP remain elusive. Various studies using GFAP knockout or transgenic mice have provided some insights

into the contribution of this protein in astrocyte physiology and pathology. GFAP plays very diverse roles in cell migration and motility[41], in mitosis by regulating filament assembly required for cytokinesis[42,43] or in vesicle trafficking, including the movement of vesicles for exocytosis, vesicle recycling, and lysosome-mediated autophagy[44,45]. Furthermore, GFAP is also suggested to be involved in the modulation of synaptic plasticity, by regulating the trafficking and the membrane anchoring of glutamate transporters[46,47], in the maintenance of the blood-brain barrier and normal CNS myelination[48].

Studies using GFAP-null ($GFAP^{-/-}$) mice have demonstrated that, despite all the cellular processes that this protein has been implicated in, GFAP is not essential in mice. GFAP-null mice displayed normal development, growth, fertility, and lifespan. When compared to wild-type mice, unchallenged GFAP-null mice showed no differences in brain architecture, and the blood-brain barrier was also intact[49-51]. However, mice deficient for GFAP, displayed an increased fragility of the CNS when subjected to head injury, which suggests that GFAP plays an important role in neural protection. Some reports suggest that the apparently innocuous phenotype displayed by $GFAP^{-/-}$ mice is due to a redundancy in the function of intermediate filaments, as other intermediate filaments like vimentin or nestin could be compensating for the absence of GFAP[53].

In response to CNS injury and disease, astrocytes undergo a complex process called astrogliosis that is characterized by an increase in the number of astrocytes, profound morphological and neurochemical changes in astrocytes, and an increase in the expression of GFAP[54,55]. The cellular and molecular mechanisms that lead to astrogliosis are not completely understood, but neuroinflammatory pathways like the Janus Kinase/Signal Transducer and Activator of Transcription 3 (JAK/STAT3) signaling pathway appear to trigger astrogliosis. The activation of astrocytes can be induced by several cytokines such as ciliary neurotrophic factor (CNTF), leukemia inhibitory factor (LIF) or interleukine-6 (IL-6), produced and secreted by damaged cells and microglia in the CNS[56,57]. Mutations or overexpression of GFAP over a toxic threshold can cause a lethal neurodegenerative disease known as Alexander disease[58].

1.3. Alexander Disease is caused by point mutations in GFAP

Alexander Disease (AxD), described by Stewart Alexander in 1949, is a rare, fatal and progressive neurodegenerative disorder that most frequently affects newborns and infants. The first report of AxD described the case of an infant who died at 16 months of age after a several-month history of severe developmental delays, regressions in cognitive and motor skills, seizures and progressive macrocephaly[59]. According to the only population-based survey ever conducted, this disease has a prevalence of 1 in 2.7 million[60], although Messing *et al.*[58] believe this number is an underestimate because symptoms are common to other disorders and often difficult to identify without previous clinical experience with this disorder. The disease occurs in both sexes, and there seems to be no predilection for race or ethnicity[58,61].

The most common classification divides patients into three subtypes based on the age of onset: infantile (0-2 years), juvenile (2-12 years) and adult (>12 years)[62]. More recently, different classifications that rely on the distribution of lesions and clinical presentations rather than age of onset have been proposed. One of these alternative systems divides patients into two categories, type I and type II, with all type I cases being early-onset, and type II cases occurring at all ages[63]. Early-onset patients normally display a very different set of symptoms than late-onset patients. Early-onset patients have a prominent frontal-lobe involvement and typical symptoms include cognitive and motor developmental delays, megalencephaly, seizures, and hyperreflexia or spasticity. Patients with later onsets more often exhibit

hindbrain dysfunction and typically experience pseudobulbar symptoms such as ataxia, dysarthria and dysphonia, sleep disturbances and very rarely have megalencephaly or seizures[58,61-63]. Lifespan is related to age of onset with type I patients having a mean survival of 14 years and type II patients of 25 years[58,61,63].

The genetic basis for AxD was defined in 2001 when Brenner and colleagues[64] reported the presence of *de novo* mutations in 4 different GFAP residues in 10 unrelated AxD patients. At the moment, GFAP is the sole known cause of AxD, with approximately 95% of patients harboring mutations in the GFAP gene[65]. In the majority of cases, GFAP mutations are not inherited but arise spontaneously. All mutations detected so far are heterozygous and about 90% of these involve single amino acid changes, though insertions and deletions have also been reported[66]. Disease-causing mutations are only known to occur in the rod and tail domains of GFAP, with most of these mutations residing in the 1A, 2A and 2B segments of the conserved central rod domain of GFAP (**Figure 1.4**). Two mutation hotspots affecting amino acids R79 and R239 (equivalent to mouse GFAP R76 and R236, respectively) account for ~ 20% of all reported cases of AxD. These two missense mutations produce the greatest variety of substitutions and cause a particular severe disease[61,63-67].

AxD is genetically dominant and mutations appear to act in a gain-of-function manner, as GFAP-null mice display a phenotype that does not resemble AxD[49-51]. However, it is still unclear if this mechanism is due to a gain of a normal function or gain of an abnormal function of GFAP. Analysis of various cases of AxD show that there is considerable phenotypic variability between affected individuals as (1) individuals with the same mutation display differences in severity of disease, (2) some patients with disease-causing mutations do not display symptoms, and (3) in rare cases of pathologically proven AxD, no mutation in GFAP has been found. The reasons for this variability are still unknown but some suggest that genetic modifiers and environmental factors may influence the appearance of disease symptoms[61,68].

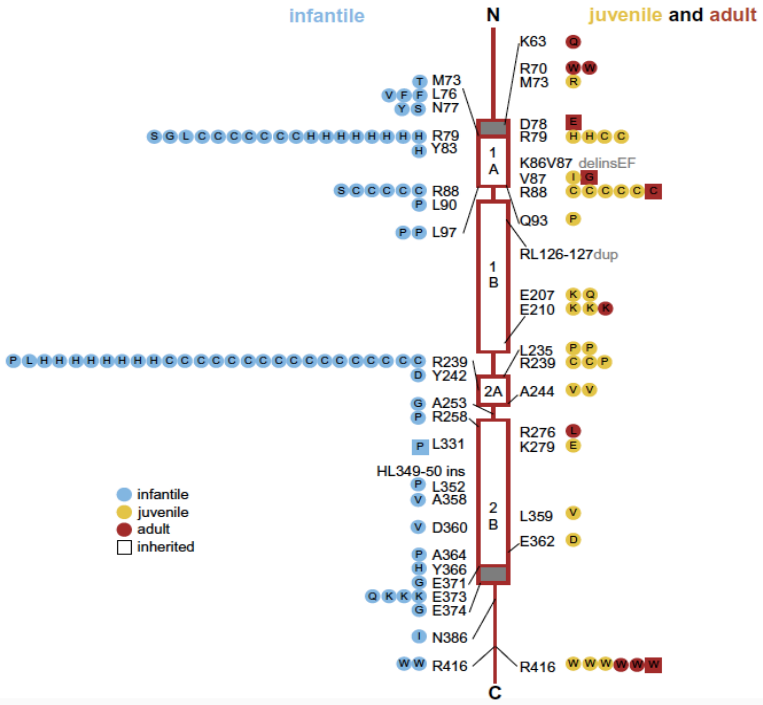

Figure 1.4: Distribution of Alexander disease-related mutations in GFAP in relation to protein domain structure of IFs and clinical presentation. Aminoacids R76 and R239 are two mutation hotspots that account for approximately 20% of all the AxD cases. These two missense mutations produce the greatest variety of substitutions and cause a particular severe disease. Adapted from [61].

An increase in GFAP levels beyond a toxic threshold, triggered by the presence of mutant GFAP, leads to the formation of eosinophilic protein inclusions known as Rosenthal fibers (RFs) (**Figure 1.5A**). These cytoplasmic inclusions mainly contain GFAP and vimentin intermediate filaments in association with stress-related proteins like alpha-β-crystallin[69] and the small heat shock protein hsp27[70], as well as other proteins in varying amounts[71]. The sequestration of both alpha-β-crystallin and hsp27 in GFAP aggregates will most likely diminish the ability of astrocytes to cope with stress[72,73] and prevent apoptosis[74]. RFs can be formed throughout the astrocyte and are thought to be generated by the continuous incorporation of small aggregates into larger inclusions, a process that continues to happen over time in parallel with the accumulation of GFAP (**Figure 1.5B**)[75]. Although RFs are characteristic of AxD, they can sometimes be found in other pathological contexts like glial scars[76] or pilocytic astrocytomas[77]. However, their numbers and distribution in AxD are noticeably higher than in these other pathologies[68,78]. Overexpression of wild-type GFAP can also lead to the formation of RFs that are indistinguishable from the ones found in AxD patients[79]. Both these results indicate that GFAP mutations, although not required for RF formation, may accelerate the process[78].

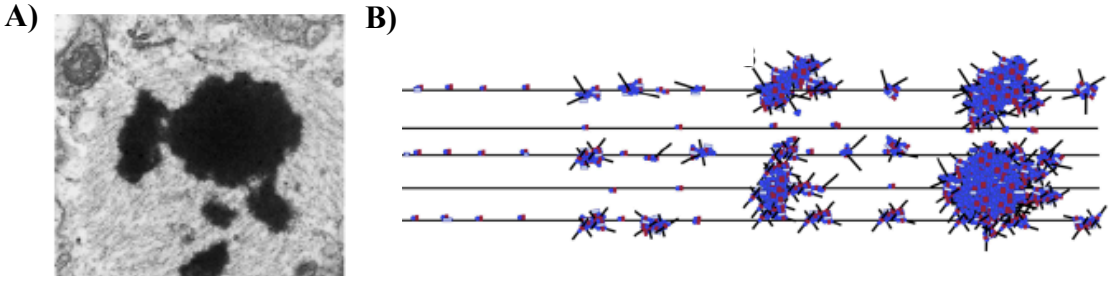

Figure 1.5: Rosenthal fibers (RFs) are the major histopathological feature of Alexander disease (AxD). (A) Morphological features of RFs. **(B)** Schematic representation of RF formation and growth. Adapted from [75].

Astrocytes in AxD display profound changes in cell shape and function, as AxD-causing mutations disturb the *in vitro* filament assembly and network formation of GFAP. When R239C GFAP was transiently expressed into Vimentin-negative SW13 cells, the protein did not form a filamentous network but instead formed small aggregates throughout the cytoplasm of cells. Although the R239C mutant also formed aggregates in primary rat astrocytes, in some of the cells it was also able to incorporate into the endogenous GFAP networks. These data suggest that GFAP mutations do not necessarily prevent GFAP assembly but could affect the ability of ULFs to anneal and subsequently compact into filaments[80,81]. Some authors propose that the effect of the mutations is to slow down the rate of normal polymer formation rather than to abolish it completely. To overcome the reduction in polymerization, astrocytes react in a self-destructive manner and increase the synthesis of mutant GFAP, resulting in a positive feedback loop for disease progression[67].

The accumulation of either wild-type or R239C GFAP in astrocytes impaired proteasome activity, but mutant GFAP produces a much stronger inhibitory effect. This proteasomal inhibition not only aggravates GFAP accumulation and aggregation, which in turn causes further proteasome inhibition but may also prevent other proteins from being degraded[81-83]. GFAP aggregation also activates a number of stress pathways such as the MAPK, p38 and JNK pathways. Constitutive activation of JNK in astrocytes leads to an increase in GFAP levels by further inhibiting proteasome activity. On the other hand, p38 activation produces the opposite effect as it negatively regulates mTOR activity, which in turn promotes

autophagy in an attempt to decrease GFAP levels[84,85]. Proteasome inhibition, and the consequent accumulation of the short-lived transcription factor Nrf2, also triggers an oxidative stress response in astrocytes marked by activation of several oxidative stress-response genes[86,87]. Furthermore, aggregates of GFAP can alter the morphology and cellular localization of some membranous organelles, like ER and Golgi, segregating these organelles to a perinuclear position. Such morphological changes may disrupt vesicle formation and consequently intracellular and membrane trafficking[75,88].

Since astrocytes play so many important roles, alterations in astrocyte function can impact other cells of the CNS. Actually, AxD astrocytes do not die, but patients show a massive white matter loss indicative of neuronal loss. One of the most characteristic changes in AxD astrocytes is the decrease of its major glutamate transporter GLT-1[89]. The loss of this transporter affects the ability of astrocytes to uptake and buffer glutamate released from synapses into the extracellular medium, which in turn can lead to neuronal hyperexcitability and death. Recent studies using both mouse and human models of AxD show that AxD astrocytes induce a strong inflammatory environment characterized by an upregulation of inflammatory genes regulated by NF-kB-mediated gene transcription, a marked activation of microglia and a modest influx of T cells into the CNS[90].

At the moment, treatments for AxD can only address symptoms, but several strategies for therapy have been proposed[91]. One approach is to screen libraries of drugs or compounds to reduce the accumulation of GFAP, either by regulating the activity of the GFAP promotor or by increasing its degradation[92]. For example, the IL-6 family of cytokines induces GFAP expression by means of the JAK/STAT3 and/or MAPK pathways. Specific targeting of these or other cytokines or rate-limiting events in these pathways could be achieved by means of drugs, gene therapy or immunotherapy (with intrabodies, for example). Another possible approach is to minimize downstream effects of GFAP toxicity, such as the deficit in the expression of the glutamate transporter GLT-1[93-95]. Enhancing protective stress responses such as those involving Nrf2[96,97] or alpha-β-crystallin[98] could also be a promising target.

2. Aims of the project

Despite the knowledge we already have on GFAP, the spatio-temporal dynamics of this protein as well as the mechanisms by which GFAP mutations lead to astrocyte dysfunction remain poorly understood. This is due, at least in part, to the difficulties in visualizing this intermediate filament *in vivo*. These difficulties arise from the fact that GFAP does not tolerate well the presence of fluorescent tags in its N- or C- termini since they are deleterious for filament assembly and lead to aggregation of the protein.

With this in mind, the overall aim of this thesis is to develop new molecular tools to study GFAP location, oligomerization and dynamics in living cells without compromising its assembly and function. Our specific objectives are:

1) Creating a new, more versatile tool for the study of mouse GFAP behavior by super-resolution microscopy or other advanced methods; and
2) Developing the first tagged version of human GFAP for the study of its behavior in normal and AxD-related conditions.

3. Material and Methods

3.1. Reagents

Cloning enzymes were purchased from Thermo Scientific (Waltham, MA, USA) unless otherwise indicated. Exceptions include *SrfI* (New England Biolabs, Ipswich, MA, USA), PfuTurbo DNA polymerase (Agilent, Santa Clara, CA, USA) and *DpnI* and alkaline phosphatase (NZYTech, Lisbon, Portugal). Cell culture media (Dulbecco's Modified Eagle Medium - DMEM - and Leibovitz's L-15 medium), Fetal Bovine Serum (FBS), penicillin-streptomycin commercial antibiotic mixture (Pen-Strep), L-glutamine, TrypLE Express dissociation reagent, Ca^{2+}- and Mg^{2+}-free phosphate buffer saline (PBS) 1X and Leukemia inhibitory factor (LIF) were obtained from Gibco® (Waltham, MA, USA). PCR primer synthesis and DNA sequencing were performed by StabVida (Caparica, Portugal). Janelia Fluor 646 nm (JF646) and Janelia Fluor 549 nm (JF549) HaloTag ligands were obtained from Promega Corporation (Madison, WI, USA) and the photoactivatable Janelia Fluor 549 nm (PA-JF549) HaloTag ligand was a kind gift from Dr. Luke Lavis (HHMI's Janelia research campus, Ashburn, VA, USA). Nocodazole was acquired from TargetMol (Wellesley Hills, MA, USA) and Latrunculin B from Focus Biomolecules (Plymouth Meeting, PA, USA). J147 and CNB-001 drugs were a kind gift from Dr. David Schubert (The Salk Institute for Biological Studies, LA Jolla, CA, United States). The following antibodies were used: rabbit anti-GFAP (1:1000, Sigma-Aldrich, St. Louis MO, USA), mouse anti-GADPH (1:2000, Santa Cruz Biotechnologies, Inc., Dallas, TX, USA), goat anti-rabbit IgG-Horseradish Peroxidase (HRP) conjugate (1:10000, Invitrogen, Carlsbad, CA, USA) and goat anti-mouse IgG-HRP conjugate (1:10000, Bio-Rad Laboratories, Hercules, CA, USA). Chemiluminescent HRP substrate was purchased from Bio-Rad Laboratories (Hercules, CA, USA). Human glioblastoma U251 cells were obtained from Public Health England (Salisbury, UK). The pEGFP-N3-mGFAP plasmid was a kind gift from Dr. Cécile Leduc (Institut Pasteur, Paris, France), the pZH504 Halo-Cro plasmid was kindly gifted by Dr. Zach Hensel (ITQB, Oeiras, Portugal) and the pcDNA3.1-EGFP-hGFAP plasmid encoding the human GFAP was developed at our laboratory by Ricardo Letra-Vilela.

3.2. Plasmid construction and site-directed mutagenesis

All plasmids were constructed using the conventional restriction digestion and ligation cloning technique. Vector and insert DNA fragments were obtained by restriction digestion of a host plasmid and through PCR amplification using Phusion polymerase, respectively.

3.2.1. Construction of a mouse GFAP-HaloTag fused plasmid

For the mGFAP-HaloTag construct, the host vector was obtained by substitution of the EGFP tag from a pEGFP-N3-mGFAP plasmid for a HaloTag using *BamHI* and *NotI* restriction sites (**Figure 3.1A**). We initially used the restriction enzymes *BamHI* and *XbaI*, but the double digestion failed. When we separately single-digested the host plasmid with each restriction enzyme, *BamHI* was able to cleave its recognition site and produce a linear plasmid, but when we tried to digest with *XbaI* the digestion was not successful due to the methylation sensitivity of *XbaI* (Data not shown). To overcome this difficulty, we opted to change the pair of restriction enzymes to *BamHI* and *NotI*. Firstly, we single- and double-digested the host plasmid with *BamHI* and *NotI* and both enzymes were able to cleave the plasmid and produce two bands, one which at 720 bp, the expected size for EGFP (**Figure 3.1B**). The HaloTag was obtained by PCR-amplification of the pZH504 Halo-Cro plasmid using specific primers (**Table 3.1**) and carrying *BamHI* and *NotI* restriction sites (**Figure 3.1C lanes 2 and 3**). PCRs were done using 20 ng of template DNA, 0.2 μM of cloning primers and 200 μM of dNTPs in a total volume of 50

µl containing 1 unit of Phusion DNA polymerase and the corresponding amplification buffer. The thermocycling conditions were the following: denaturation at 98ºC for 30 s followed by 30 cycles of 98ºC, 10 s; 65ºC, 30 s; 72ºC, 30 s (30 s/kb, as specified by the manufacturer) and a final extension at 72ºC for 10 min. Insert and vector fragments were digested for 2 h at 37ºC. Digested vectors were further incubated with 0.5 units of alkaline phosphatase for 1 h at 37ºC to prevent spontaneous religation of the vector. Digested vectors were then isolated by agarose gel electrophoresis (1% in Tris-acetate-EDTA – TAE - 1X) and purified with a NZYGelpure kit (NZYTech, Lisbon, Portugal). Digested vectors and inserts were ligated for 2 h at room temperature using 5 units T4 DNA ligase. Four different molar ratios of vector: insert were used – 1:0, 1:3, 1:6 and 1:9 – with the 1:0 ratio serving as a control for non-specific vector religation. Ligation products were transformed into NZY5α competent *E. coli* bacteria (NZYTech, Lisbon, Portugal) by heat shock and grown overnight at 37ºC on LB Agar 1X Petri dishes containing 50 µg/ml of kanamycin or 100 µg/ml of ampicillin for selection of transformed clones. Two different methods were used to determine if the cloning was successful. First, plasmids from randomly chosen colonies were isolated, digested with restriction enzymes and the resulting products analyzed by agarose gel electrophoresis. As shown in **Figure 3.1D**, in all of the tested colonies, plasmid digestion with *BamHI* and *NotI* generated 2 bands, one corresponding to the linearized plasmid and another in accordance with the size of the HaloTag (891 bp). To further confirm the cloning efficacy, 3 positive clones were sequenced, and in all the presence of the HaloTag was confirmed. No insertions or deletions were observed but all the clones had a single nucleotide mutation, that did not change the amino acid sequence. This mutation was probably present in the original template for HaloTag PCR amplification.

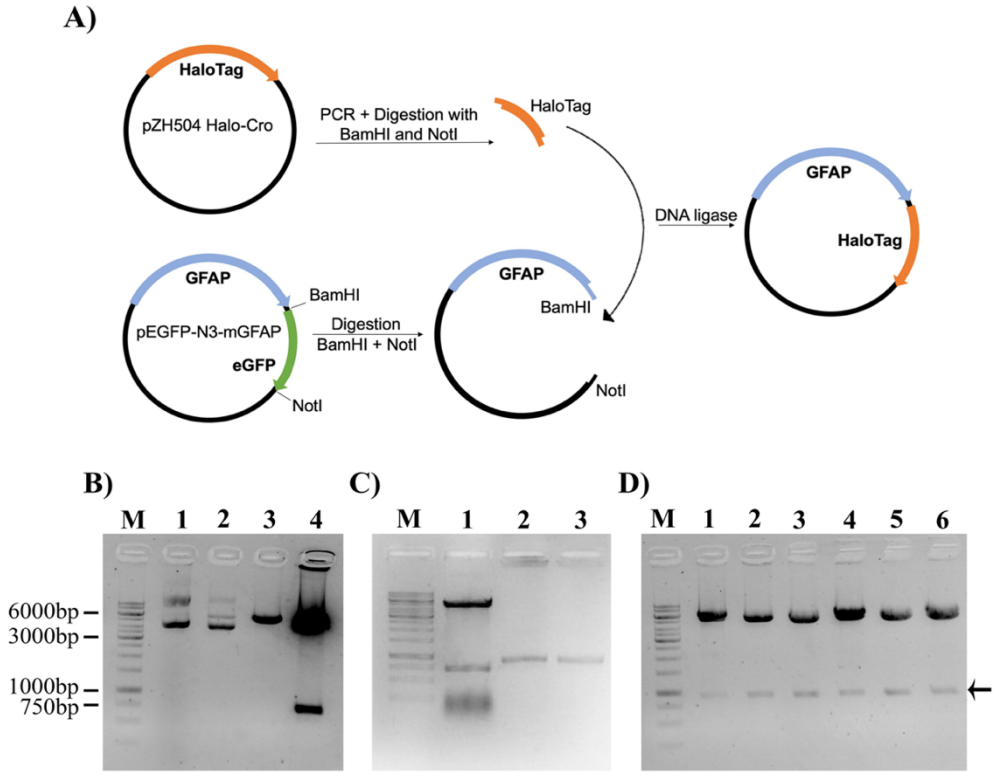

Figure 3.1: Cloning strategy for the construction of a mouse GFAP-HaloTag (mGFAP-HT) fused plasmid. (A) The HaloTag protein was amplified as a 5'BamHI-3'NotI PCR fragment and cloned into a BamHI-NotI digested pEGFP-N3-GFAP plasmid. **(B)** Test digestion of the pEGFP-N3-GFAP plasmid; M – marker; lane 1- undigested plasmid; lane 2 - Single-digestion with *BamHI*; lane 3 – Single-digestion with *NotI*; lane 4 – Double-digestion with *BamHI* and *NotI*. **(C)** Vector and insert DNA fragments used for the construction of the mGFAP-HT plasmid. Vector fragments were prepared by double-digestion of the pEGFP-N3-GFAP plasmid with *BamHI* and *NotI* (lane 1) and insert fragments were obtained by PCR-amplification of a pZH504 Halo-Cro plasmid (lanes 2 and 3). **(D)** Confirmation of correct plasmid assembly by digestion with *BamHI* and *NotI* restriction enzymes. Positive clones are indicated by an arrow.

3.2.2. Construction of tagged human GFAP constructs

All cloning procedures were done as described in the previous subsection. Human GFAP constructs were obtained by substitution of the EGFP tag in our in-house pcDNA3.1-EGFP-hGFAP plasmid by Venus 1 (amino acids 1-157), Venus 2 (amino acids 158-238) or full-length HaloTag inserts. For these operations, we used the restriction enzymes *AscI* and *SrfI*. The Venus 1, Venus 2 and HaloTag inserts were amplified as 5'AscI – 3'SrfI PCR fragments using a pCS2-Venus or the pZH504 Halo-Cro plasmids as templates and the primers described in **Table 3.1**.

3.2.2. Site-directed mutagenesis

Single p. Arg236His (R236H) and p. Arg239Cys (R239C) mutations were individually inserted by site-directed mutagenesis into the wild-type mGFAP and hGFAP constructs, respectively. PCRs were carried out using 25 ng of template DNA, 0.2 μM of mutagenesis primers (**Table 3.1.**) and 250 μM of dNTPs in a total volume of 50 μl containing 2.5 units of *Pfu turbo* DNA polymerase and the corresponding amplification buffer. The following thermocycling conditions were used: denaturation at 95ºC followed by 12 cycles of 95ºC, 30 s; 55ºC, 1 min; 68ºC, 8 min (1 min/kb, as specified by the manufacturer) and a final extension at 68ºC for 5 min. Mutagenesis reactions were then incubated with *DpnI* for 1 h at 37ºC to digest methylated parental plasmids and later transformed by heat shock into NZY5α competent bacteria. Transformed bacteria were grown overnight at 37ºC on LB Agar 1X Petri dishes with 50 μg/ml of kanamycin or 100 μg/ml of ampicillin for selection. Plasmids from randomly chosen colonies were isolated using a ZYMO Research Miniprep kit and sequenced to confirm the presence of the mutations.

Table 3.1: Sequences of primers (5' → 3') used to construct plasmids encoding tagged GFAP or in site-directed mutagenesis of these constructs

Construct	Primer sequence (5' → 3')
mGFAP - HaloTag	Forward: AATGGATCCATGGCAGAATCGGTACTGGC Reverse: TATGCGGCCGCTTAGCCGGAAATCTCGAG
hGFAP - Venus 1	Forward: AATGGCGCGCCATGGTGAGCAAGGGCG Reverse: AATGCCCGGGCTTGCTTGTCGGCGGTGAT
hGFAP – Venus 2	Forward: AATGGCGCGCCAAGAACGGCATCAAGGC Reverse: AATGCCCGGGCGTACAGCTCGTCCATGC
hGFAP - HaloTag	Forward: AATGGCGCGCCATGGCAGAAATCGGTAC Reverse: ATAGCCCGGGCGCCGGAAATCTCGAGC
Arg236His (R236H)	Forward: CTGAGAGAGATTCACACTCAATACGAG Reverse: CTCGTATTGAGTGTGAATCTCTCTCAG
Arg239Cys (R239C)	Forward: CTGAAAGAGATCTGCACGCAGTATG Reverse: CATACTGCGTGCAGATCTCTTTCAG

3.3. Cell culture

3.3.1. Cell growth, seeding and transfection

Human glioblastoma U251 cells and rat glioma C6 cells were grown to confluence in 100 mm dishes (Thermo Scientific, Waltham, MA, USA) in DMEM, supplemented with 10% (v/v) fetal bovine serum (FBS), 1% (v/v) Penicillin-Streptomycin and 1% (v/v) L-glutamine and maintained at 37ºC in a humidified atmosphere containing 5% CO_2. Medium was changed every other day and cells were passed once a week by trypsinization. Briefly, cells were incubated with TrypLE Express dissociation reagent for 5 min at 37ºC for cell detachment, followed by a centrifugation step at 300 g for 5 min at room temperature and sub-cultured according to the desired dilution. For fluorescent microscopy and single-molecule tracking experiments, 3×10^5 cells were grown on 35 mm glass-bottom μ- dishes (21 mm glass surface diameter, ibidi GmbH, Gräfelfing, Germany). For flow cytometry, 3×10^5 cells were seeded on 6-well plates (35 mm diameter, Corning®, Corning, NY, USA). For Western blotting, 8×10^5 cells were seeded on 60 mm dishes (Orange Scientific, Braine-L'Alleud, Belgium). Twenty-four hours after seeding, cells were transiently transfected with 1 μg of the corresponding DNA constructs using jetPRIME® transfection reagent (Polyplus transfection, Illkirch, France) in a proportion of 3:1 (μL of transfection reagent: μg of DNA).

3.3.2. Drug treatments and cell labeling

All drugs and HaloTag ligands were diluted in DMSO (100% v/v). To test the neuroprotective activity of J147 and CNB-001, cells were treated with 100 nM, 1 μM or 10 μM of each drug 20 min before transfection and incubated for 24 h at 37ºC. For single-molecule experiments, 24 h after transfection, serum was removed for 2 h, and cells were treated with LIF (100 ng/ml), Nocodazole (10 μM) or Latrunculin B (10 μM) for 2 h at 37ºC in serum-free medium. Cells were then incubated with JF646 (100 nM), JF549 (100 nM) or PA-JF549 (1 nM) HaloTag ligands in serum-free medium for 20 min at 37ºC. Subsequently, cells were washed twice with sterile PBS. At the end of the final wash, the medium was changed to Leibovitz's L-15 without phenol red.

3.4. Microscopy

Live-cell images of U251 cells were acquired at Instituto Gulbenkian de Ciência on a commercial widefield Nikon High Content Screening microscope, equipped with a 100x/1.45 plan-apo oil-immersion objective and an Andor Zyla 4.2 Scientific complementary metal-oxide-semiconductor (sCMOS) camera. To image eGFP/Venus–fused proteins, a 470 nm laser line, and GFP fluorescence filter sets were used and for the imaging of HaloTag-fused proteins, a 635 nm laser line and Cy5 fluorescent filter sets were used. An exposure time of 80 ms was used and the camera readout bandwidth was set to 200 MHz. The resulting pixel size was 65 nm using a 1024 x 1024 pixel as field of view. All acquisitions were done at room temperature. The microscope, cameras, and hardware were controlled through Nikon Elements software. Images were analyzed by means of the ImageJ free software.

Single-molecule imaging and Super-Resolution Radial Fluctuations (SRRF) imaging were performed on a Leica DMI6000 inverted microscope using a 100x/1.46 a-plan apochromat oil immersion objective. A 561 nm excitation laser (Coherent Sapphire) was set to 50 mW resulting in an effective power density of ~ 2.3 kW/cm^2. The laser beam was passed through a custom filter cube (Chroma Technology) with a zet405/561x excitation filter, a zt405/561/657rpc-uf2 dichroic beamsplitter, and an et610/75m emission filter. Fluorescent light was imaged on an Evolve 512 electron-multiplying charge-coupled device (EM-CCD) camera (Photometrics) after additional 1.6x magnification. An EM gain of

300 was used and the camera readout bandwidth was set to 10 MHz. The resulting pixel size was 100 nm using a 512 x 512 pixel as field of view. The incubation chamber was maintained at 37°C. The microscope, cameras, and hardware were controlled through MetaMorph software (Molecular Devices). For single-molecule experiments and for each cell, 1000 frames were acquired at 33 ms exposure time with no interval between frames. No photoactivation was necessary as spontaneous photoactivation of PA-JF549 combined with photobleaching by 561 nm illumination gave a reasonable density of single molecules. The Trackmate ImageJ plugin[99] was used to detect, fit and track individual GFAP molecules in living cells. For the detection of GFAP molecules, we selected a LoG detector and an estimated blob diameter of 0.4 μm and a threshold of 1500. For the tracking, we used a simple LAP tracker with a linking max. distance of 0.5 μm, a gap-closing max. distance of 0.5 μm and a gap-closing max. frame gap of 0. The average diffusion of GFAP molecules and its fractions, per individual cell, were calculated by fitting the SpotOn[100] 2-state (bound-free) kinetic model (0.05 $\mu m^2/s$ as maximum D_{bound} and 0.02 $\mu m^2/s$ as minimum D_{free}) to the distribution of translocations for individual molecules, obtained with TrackMate. For SRRF imaging, 100 frames were acquired for each cell. SRRF images were generated by running the NanoJ-SRRF ImageJ[101] plugin on groups of 100 diffraction-limited images using the default settings.

3.5. Flow cytometry

Twenty-four hours after transfection with the corresponding constructs, cells were washed once with Ca^{2+}- and Mg^{2+}- free PBS and then detached with TrypLE Express dissociation reagent for 5 min at 37ºC. Complete DMEM medium was added to the cells to neutralize TrypLE, and cells were collected to a microcentrifuge tube. Cells were centrifuged at 300 g for 5 min at room temperature, the supernatant was discarded, and pellets were resuspended in PBS. Fluorescent levels were determined using a 488 nm excitation laser and a 582/42 fluorescent filter. Flow cytometry was performed at Instituto Gulbenkian de Ciência on a FACSCalibur cytometer using Cell Quest software (Beckton Dickinson, Franklin Lakes, NJ, USA). Ten thousand events per experimental group were acquired and results were analyzed using FlowJo software (Tree Star Inc., Ashland, OR, USA).

3.6. Immunoblotting

Cells were washed once with PBS 1X and then incubated with a lysis buffer (50 mM Tris-HCl, 150 mM NaCl, 1% (v/v) NP-40 pH 7,5) supplemented with a protease inhibitor cocktail (Amresco, Fountain Parkway Solon, OH, USA). Cells were collected by scraping, transferred to microcentrifuge tubes, and incubated in ice for 10 min. To release intracellular proteins, cells were sonicated for 5 s using a Sonifier W - 450 D sonicator (Emerson, St. Louis, MO, USA). Proteins were collected after cell lysate centrifugation at 10000 g for 10 min at 4ºC and quantified by means of the Bradford method. Briefly, proteins were incubated with Bradford reagent (ApploChem Panreac, Cinisello Balsamo, Milan, Italy) for 10 min in the dark before measuring the absorbance at 595 nm. Protein concentrations were calculated by means of a standard curve of known bovine serum albumin (BSA) concentrations (0.125 to 2 μg/μL). For SDS-PAGE immunoblotting, 25 μg of total protein extracts were mixed with 4X loading buffer (4% (v/v) sodium dodecyl sulfate (SDS), 10% (v/v) 2- mercaptoethanol, 20% (v/v) glycerol, 0.004% (v/v) bromophenol blue, 0.125 mM Tris-HCl, at pH 6,8), boiled at 95ºC for 5 min to denature proteins, and incubated on ice for 5 min. Protein samples were separated by electrophoresis using a 10% (w/v) SDS-polyacrylamide gel and run at 125 V for 1 h. Proteins were transferred to a nitrocellulose membrane at 100 V for 1 h. Membranes were stained with 0.1% (w/v) Ponceau S to confirm sample quality and then washed with Milli Q water and Tris-HCl buffer saline (TBS) (150 mM NaCl, 50 mM Tris pH 7,4).

Membranes were subsequently blocked with 5% (w/v) non-fat dry milk in Tris-HCl buffer saline-Tween solution (TBS-T) (0.5% Tween-20) for 1 h at room temperature. After 3 washing steps with TBS-T, membranes were incubated with primary antibodies (diluted in 3% (w/v) BSA, 0.05% (v/v) sodium azide (NaAZ) in TBS-T) against GFAP (1:1000) and GAPDH (1:2000) overnight at 4ºC in a rotating wheel. To remove unbound antibody, membranes were rinsed 3 times with TBS-T for 10 min followed by an incubation with a secondary HRP-conjugated antibody (1:10000) in 5% (w/v) non-fat dry milk, for 2 h at room temperature with agitation. Membranes were rinsed 3 times for 10 min with TBS-T, incubated with chemiluminescent HRP substrate and imaged in a ChemiDoc XRS+ system (Bio-Rad, Hercules, CA, USA).

3.7. Statistical analysis

Statistical analysis and graphical representation of data were performed using Sigmaplot software (Systat Software, Inc., San Jose, CA, USA). Sample data are represented as mean ± standard deviation (SD) of at least 3 independent experiments. Statistical significance was evaluated by means of a one-way ANOVA followed by a Tukey's test. Results were considered significant when $p < 0.05$, but in some cases, we also specified lower significance thresholds ($p<0.01$; $p<0.001$).

4. Results

Green fluorescent protein (GFP) and its spectral variants are versatile biological markers that have significantly changed our ability to study protein localization, dynamics, and interactions in living cells[102,103]. However, these fluorescent proteins also have several disadvantages, including their low photostability and brightness when compared to organic dyes, the potential formation of homo-oligomers and limited choices in spectral wavelengths[104,105]. Due to these biophysical and photophysical properties, fluorescent proteins are often inadequate for super-resolution microscopy. An attractive alternative approach is the use of self-labeling protein tags, such as the HaloTag[106], a hybrid approach that combines the genetic specificity of fluorescent proteins with the superior photophysics of organic dyes. The HaloTag is a genetically engineered derivative of a hydrolase that, in physiological conditions, efficiently forms a highly specific and irreversible covalent bond with a multitude of synthetic chloroalkane ligands, including a variety of spectrally distinct fluorescent tags, affinity tags, and attachments to solid supports.

4.1. Mouse GFAP-HaloTag fused plasmid is successfully expressed in U251 cells

We started by testing the effect of expressing a mGFAP-EGFP construct in U251 human glioblastoma cells and C6 rat glioma cells by transient transfection. This construct was able to incorporate into the endogenous IF network and form a normal filamentous pattern when expressed in U251 cells (**Figure 4.1A**), but not in C6 cells (**Figure 4.1B**), reflecting that the behavior of GFAP is not universal and depends on the cellular context.

In order to study the architecture and behavior of GFAP at a nanoscopic level in living cells, we constructed a mouse-GFAP-HaloTag (mGFAP-HT) plasmid. This plasmid, as described in the Materials and Methods section, was generated by substitution of the EGFP tag from a host pEGFP-N3-mGFAP (mGFAP-EGFP) plasmid for a HaloTag using *BamHI* and *NotI* restriction sites and keeping the molecular linker between GFAP and HaloTag. As seen in **Figure 4.1C,** our mGFAP-HT construct was also able to form a normal filamentous network similar to that of mGFAP-EGFP, when transiently expressed in U251 cells. Furthermore, the application of the SRRF algorithm to the widefield images of mGFAP-HT was able to reconstruct these diffraction-limited low-resolution images into high-resolution images and provide higher resolution details about the architecture of GFAP fibrils (**Figure 4.1D**).

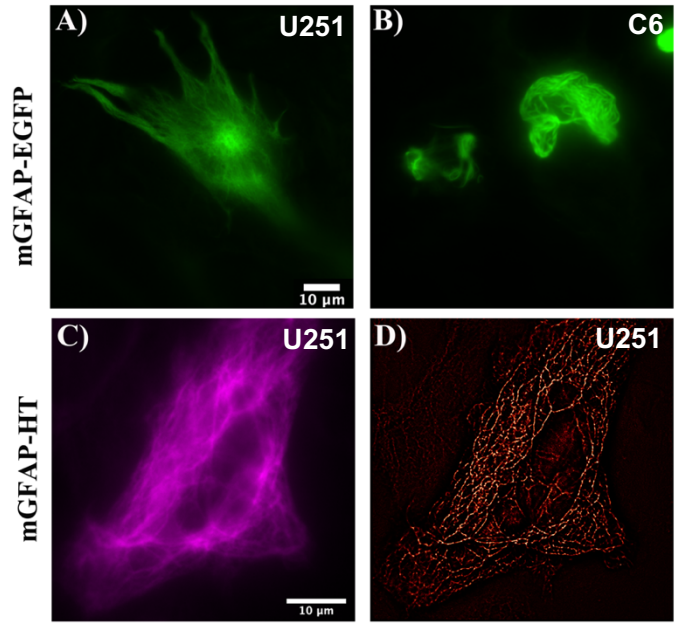

Figure 4.1: Halo mouse GFAP is successfully expressed in U251 human glioblastoma cells. mGFAP-EGFP construct exhibited a normal GFAP filamentous network, when transiently expressed in U251 cells (**A**), but not in C6 cells (**B**). (**C**) U251 cells transfected with the mGFAP-HT construct and labeled with the JF549 Halo ligand (100 nM) also displayed a normal filamentous network characteristic of GFAP. (**D**) Widefield images of the mGFAP-HT construct were further analyzed with the NanoJ Super-Resolution Radial Fluctuations (SRRF) algorithm, which provided higher resolution details about the GFAP fibrils. Scale bars - 10 µm.

4.2. Alexander disease-causing mutation R236H is deleterious to the assembly and network formation of mouse GFAP

To understand the effect of AxD-causing mutations on the assembly properties of GFAP, a R236H AxD-mutant was generated by site-directed mutagenesis. Transient transfection of WT mGFAP into U251 cells resulted in its incorporation within the endogenous IF network and in the formation of filament networks (**Figure 4.2A, left panel)** in approximately 87% of the transfected cells (**Figure 4.2B**). A diffuse homogeneous pattern or an aggregation pattern was occasionally observed in 11% and 2% of the transfected cells, respectively (**Figure 4.2B**). In contrast, transient expression of the R236H AxD-mutant disrupted the endogenous GFAP network, as the majority of the cells did not display an obvious filamentous structure (**Figure 4.2A, right panel**). Instead, GFAP either distributed homogeneously throughout the cytoplasm (45% of the cells) or formed cytoplasmatic inclusions (15% of the cells) (**Figure 4.2B**).

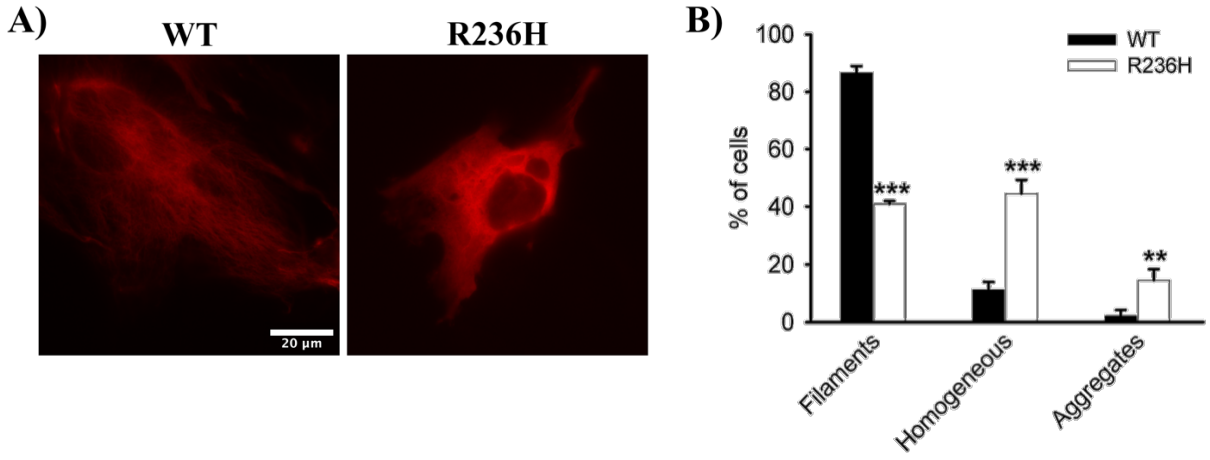

Figure 4.2: Alexander disease-related R236H mutation causes filament disorganization of GFAP. U251 cells were transiently transfected with either WT or mutant R236H GFAP, and 24 h later labeled with the JF646 Halo ligand (100 nM). **(A)** When expressed in this cell line, WT GFAP assembled into filaments (left panel), but mutant GFAP mostly formed a homogeneous pattern throughout the cytoplasm without any apparent filament structures (right panel). **(B)** Quantification of the various patterns observed for transfected U251 cells with WT GFAP (black bars) and mutant GFAP (white bars). Results are shown as mean ± SD of triplicates. * significant versus WT GFAP. ** $p<0.01$, *** $p<0.001$. Scale bar – 20 µm.

We next analyzed the dynamics of the mGFAP-HT construct using single-molecule tracking, a powerful method to probe the mobility of molecules in living cells[107]. Images from living cells labeled with the fluorescent HaloTag ligand PA-JF549 were acquired to generate 2D single-molecule tracks of the movement of each GFAP molecule. GFAP molecules do not have all the same diffusion motion, and we can clearly distinguish between molecules that have limited dynamics (**Figure 4.3A and 4.3B, circle**), and molecules exhibiting rapid diffusion or directional motion (**Figure 4.3A and 4.3B, arrow**). To evaluate quantitatively the diffusive properties of GFAP we used the Trackmate ImageJ plugin to detect, localize and fit and track individual molecules. As observed in **Figure 4.3C** this plugin was able to detect with high accuracy the different GFAP molecules, in each frame. The individual tracks obtained were exported directly into the web-interface Spot-On and it was assumed that GFAP molecules could be distributed into 2 distinct subpopulations: a slow diffusion population and a rapid diffusion population. The Spot-On model does not account for directional motion or confined diffusion but was sufficient to provide a good fit for diffusion jump distributions for single-cell data.

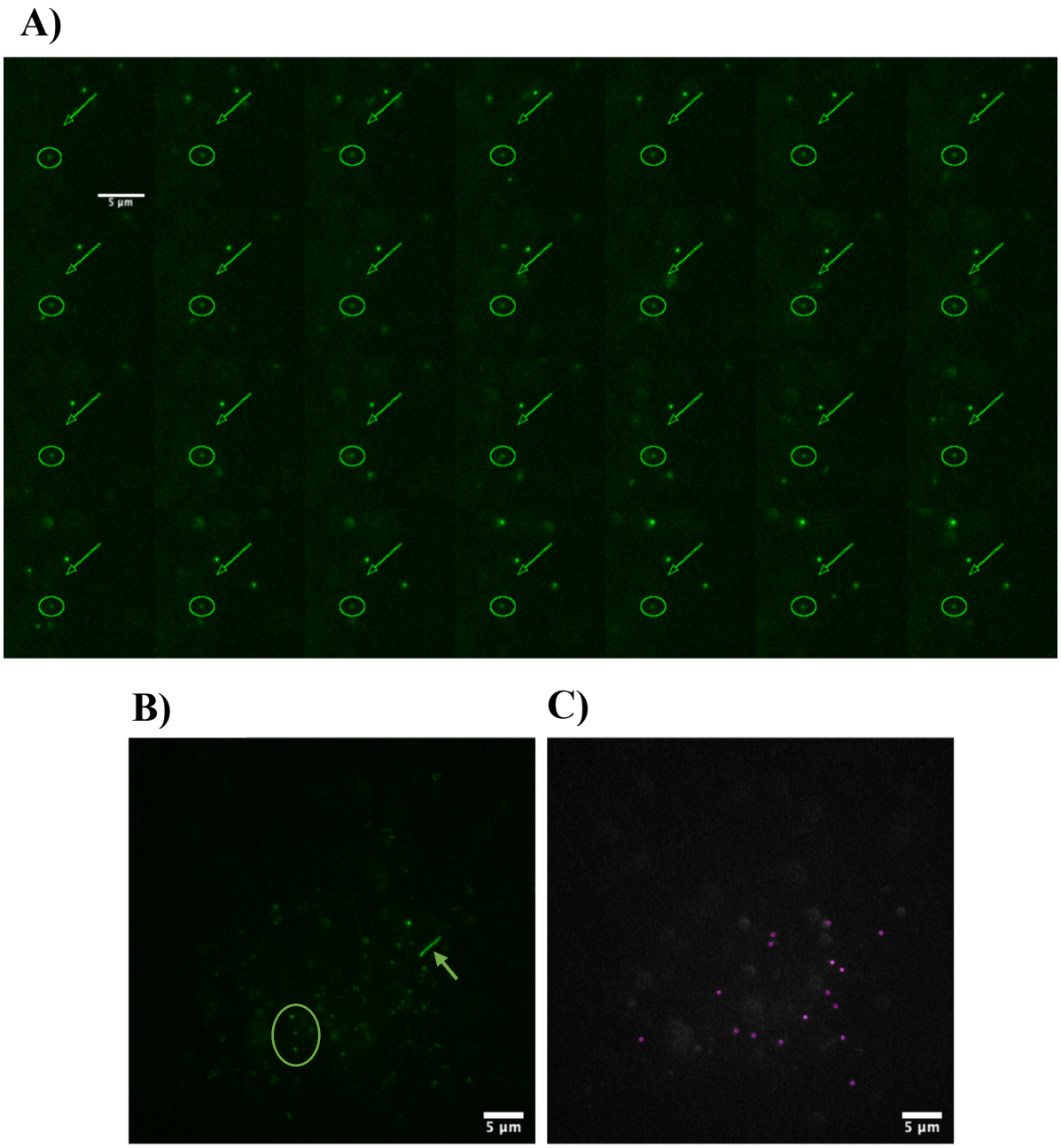

Figure 4.3: GFAP molecules display different diffusion behaviors. (A) Different types of diffusion motion of GFAP molecules. arrow – fast-diffusing molecule; circle – slow-diffusing molecule. **(B)** Z-stack projection of the different diffusion motions of GFAP molecules. arrow – fast-diffusing molecule; circle – slow-diffusing molecules. **(C)** Detection of GFAP molecules with the Trackmate ImageJ plugin. Scale bars – 5 µm.

Spot-On analysis of the R236H mutant demonstrated that this mutation has a strong effect on the dynamics of GFAP molecules, and results in a significant increase in the rate of diffusion when compared to the WT (from ~ 0.13 $\mu m^2/s$ to ~0.21 $\mu m^2/s$) (**Figure 4.4A**). However, the fraction of slow-diffusing R236H GFAP molecules does not differ from WT (**Figure 4.4B**). To further characterize the dynamics of GFAP, cells were treated with either LIF (100 ng/ml) to activate endogenous GFAP expression, nocodazole (10 μM), an antineoplastic agent that interferes with the polymerization of microtubules or latrunculin B (10 μM), a drug that disrupts actin filaments. Results revealed that the increase in GFAP expression by LIF had little effect on the diffusion of GFAP molecules (**Figure 4.4C**), but increased, slightly, the fraction of slow-diffusing molecules (**Figure 4.4D**). Conversely, destabilization of the actin and microtubules networks significantly decreased the diffusion of GFAP molecules (**Figure 4.4C**) and increased the fraction of slow-moving molecules (**Figure 4.4D**), which emphasizes the importance that actin filaments and microtubules have on the dynamics and maintenance of the GFAP network.

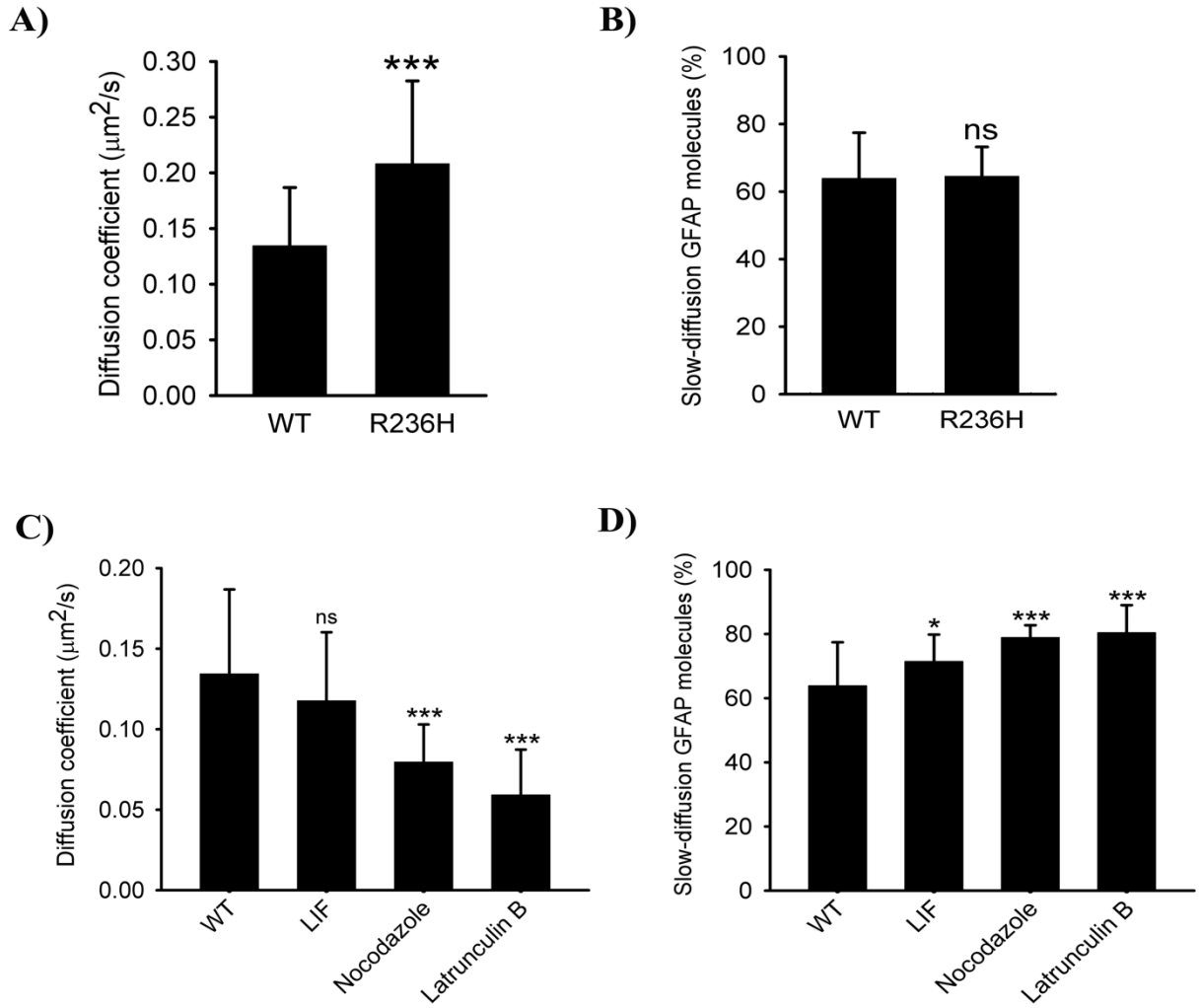

Figure 4.4: AxD-related R236H mutation alters the diffusion properties of mGFAP. (A) Average diffusion coefficient ($\mu m^2/s$) of rapid-diffusing molecules and **(B)** fraction (%) of slow-diffusing GFAP molecules calculated for individual cells by Spot-On for WT GFAP (20 cells) and R236H mutant (20 cells). **(C)** Average diffusion coefficient ($\mu m^2/s$) of rapid-diffusing molecules and **(D)** fraction (%) of slow-diffusing GFAP molecules calculated for individual cells by Spot-On for WT GFAP untreated (20 cells) and treated with LIF (100 ng/ml, 20 cells), Nocodazole (10 μM, 20 cells) or Latrunculin B (10 μM, 20 cells). Results are shown as mean ± SD. ns – non-significant; * significant versus WT GFAP. * $p<0.05$, *** $p<0.001$.

4.3. Generation of tagged human-GFAP constructs

Previously, we generated a human-GFAP-EGFP (hGFAP-EGFP) fused construct by randomly inserting the coding region of EFGP into the coding region of hGFAP, following a technique described elsewhere[108]. Briefly, in the presence of a transposase protein, a 1902 bp transposon containing the coding region for EGFP and kanamycin resistance (Kan^r) was inserted, randomly, into a pcDNA3.1/Ampicillin (Amp^r) resistant target plasmid containing the coding region for human GFAP. Successfully transposed plasmids carried both Amp^r and Kan^r as selection markers (**Figure 4.5A**). The transposon insertion was confirmed by PCR-based colony screening using primers specific for GFAP. Positive colonies were then digested with *Srf1* to remove the Kan^r region, and the resulting plasmids were transfected into U251 cells and tested for fluorescence by means of flow cytometry and fluorescence microscopy.

Using the hGFAP-EGFP fused plasmid and the same cloning strategy described previously in Section 3.2.1, we generated two new hGFAP constructs by substituting the EGFP tag of the hGFAP-EGFP plasmid for a Venus 1 (amino acids 1-157) or Venus 2 (amino acids 158-238), in order to create a Biomolecular Fluorescent Complementation (BiFC) system (**Figure 4.5B**). BiFC systems are an important tool to visualize and study protein-protein interactions in living cells. The BiFC is a two-plasmid system where the proteins of interest, in our case human GFAP, are fused to either the N-terminal half (V1) or the C-terminal half (V2) of the Venus fluorescent protein. These Venus fragments are not fluorescent by themselves. However, if the proteins of interest interact, the Venus halves come together, reconstitute the native structure of the fluorophore and emit fluorescence (**Figure 4.5C**)[109]. Such system would allow us to identify or visualize hGFAP interactors in living cells or quantify the formation of hGFAP dimers during the process of fibrillization.

When transfected into U251 cells, our hGFAP-BiFC system produced a fluorescent signal, as detected by flow cytometry, indicating the constructs were successfully expressed (**Figure 4.5D**). However, the number of fluorescent cells was very low. Fluorescence microscopy results were consistent with flow cytometry results, as only a very low number of cells were fluorescent, and they showed low fluorescence that quickly photobleached. In contrast to our hGFAP-EGFP construct, which was able to form filamentous networks typical of GFAP in both U251 (**Figure 4.5E, left upper panel**) and C6 (**Figure 4.5E, left bottom panel**), the BiFC system failed to form such networks, but instead formed aggregates with no apparent filamentous structure (**Figure 4.5E, right upper panel**). This was essentially the same result our laboratory obtained when we previously tried to create a hGFAP BiFC system adding the BiFC tags to the N- or C-termini of the hGFAP protein.

We also used our hGFAP-EGFP construct as a host vector for the generation of a hGFAP-HaloTag construct, in an attempt to reproduce our results with mGFAP (**Figure 4.5B**). Similar to the BiFC system, this construct did not form any filamentous structure in living cells labeled with the JF646 ligand (100 nM) but instead formed small aggregates dispersed throughout the cytoplasm of the cells (**Figure 4.5E, right bottom panel**). These results were the same when cells were labeled with the JF549 ligand (100 nM) (Data not shown).

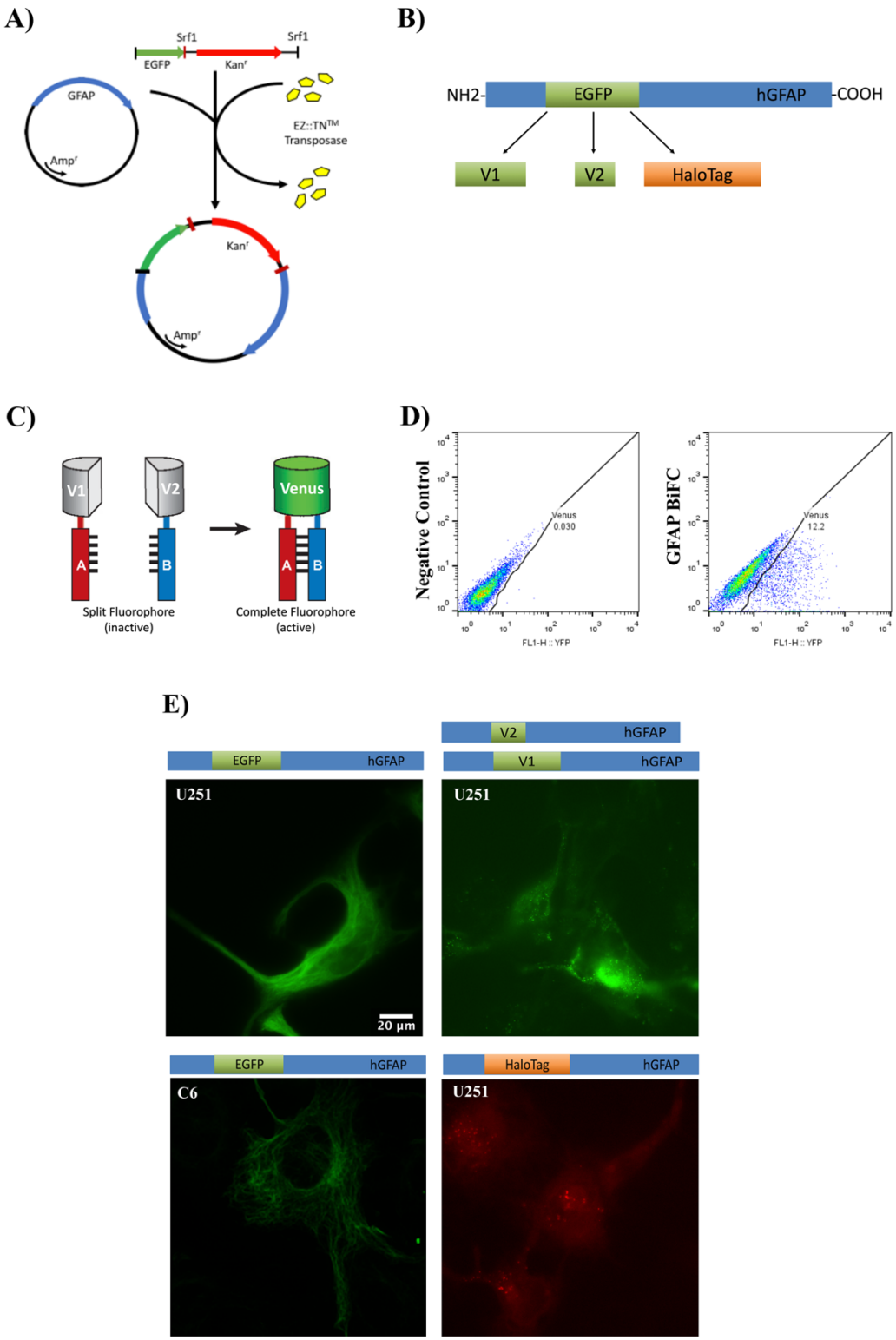

Figure 4.5: Construction of tagged human GFAP plasmids. (A) Transposon strategy to generate human GFAP-EGFP fused constructs. **(B)** Human GFAP constructs were obtained by substitution of the EGFP tag of the pcDNA3.1-EGFP-hGFAP plasmid by Venus 1 (amino acids 1-157), Venus 2 (amino acids 158-238) or full-length HaloTag. **(C)** The schematic principle of the BiFC system. **(D)** Flow cytometry charts of untransfected U251 cells (negative control, left panel) and cells transfected with the GFAP BiFC system (right panel). **(E)** Fluorescent microscopy analysis revealed that our hGFAP-EGFP construct is able to form characteristic GFAP filaments when transiently expressed in U251 cells (left upper panel) and in C6 cells (left bottom panel). In contrast, U251 cells transiently transfected with the hGFAP BiFC system (right upper panel) or with the hGFAP-HT construct and labeled with JF646 ligand (100 nM) (right bottom panel) do not display any apparent filaments, but instead, GFAP forms small aggregates throughout the cytoplasm of the cells. Scale bar – 20 µm.

4.4. Alexander disease-related R239C mutation induces human GFAP aggregation

Next, we tested the effect of expressing wild-type GFAP and the R239C mutant, generated by site-directed mutagenesis, in U251 cells. Western-blot analysis confirmed the expression of both constructs in U251 cells and revealed that GFAP levels were similar between cells transfected with WT and mutant GFAP (**Figure 4.6A**). While cells transfected with WT GFAP exhibited a typical filamentous network (**Figure 4.6B, left panel**), cells transfected with the Alexander-disease R239C mutant showed GFAP inclusions dispersed throughout the cytoplasm (**Figure 4.6B, right panel**). The pattern of aggregation and the size of the aggregates displayed by mutant GFAP varied significantly between cells, with some cells exhibiting less numerous but larger aggregates and others exhibiting a large number of small aggregates. Quantification of microscopy data revealed that about 90% of the cells transfected with WT GFAP contained filaments, while this percentage dropped to about 40% for cells transfected with the mutant form of GFAP. On the other hand, while only 3% of the cells transfected with WT GFAP showed an aggregation pattern, this percentage significantly increased to 48% for cells transfected with the R239C mutant (**Figure 4.6C**).

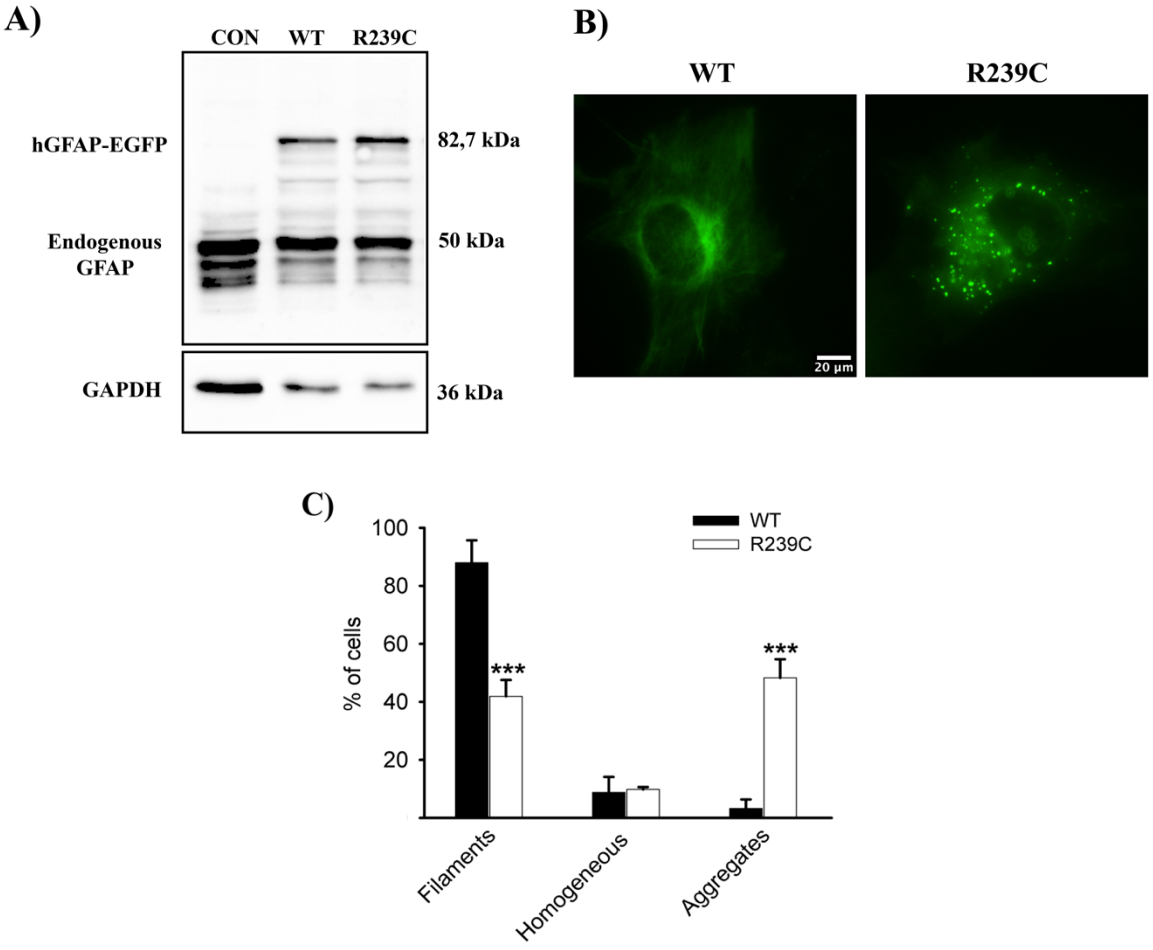

Figure 4.6: Transient expression of mutant R239C GFAP leads to aggregate formation in U251 cells. (A) U251 cells were transfected with the indicated GFAP constructs and total protein extractions were analysed by immunoblotting using an anti-GFAP antibody that recognizes both endogenous and exogenous GFAP. **(B)** Filamentous and aggregate patterns formed by WT GFAP (left panel) and R239C mutant GFAP (right panel), respectively. **(C)** Distribution of patterns after transfection of WT (black bars) and mutant (white bars) constructs into U251 cells. * significant versus WT GFAP. ***$p<0.001$. Scale bar – 20 µm.

Although there is still no treatment for AxD, several drugs and compounds targeting GFAP expression and accumulation have been screened in multiple *in vitro* cell assays. Given the reported beneficial effects of curcumin in a cellular model of Alexander disease, we sought to test the neuroprotective effect of two synthetic and improved curcumin derivatives, J147 and CNB-001, on GFAP accumulation. To this end, cells transfected with the R239C mutant GFAP were treated with 100 nM, 1 μM or 10 μM of each drug. As shown in **Figure 4.7**, only cells grown in the presence of 10 μM of CNB-001 showed a significant increase in filament formation and a corresponding decrease in GFAP aggregation.

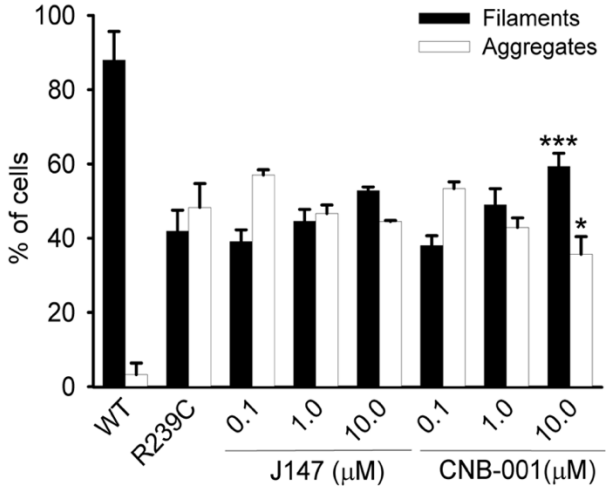

Figure 4.7: CNB-001 has a beneficial neuroprotective effect on GFAP filament organization and accumulation. Quantification of U251 cells transfected with the GFAP R239C mutant that displayed a normal filamentous network (black bars) or aggregates (white bars) after treatment with increasing concentrations (0.1-10 μM) of the neuroprotective compounds J147 or CNB-001. Results are shown as mean ±SD of triplicates. All groups were statistically significant versus WT ($p<0.001$). * significant versus R239C mutant GFAP. * $p<0.05$, *** $p<0.001$.

5. Discussion

The cytoskeleton is a complex network of protein filaments and motor proteins that provides the structural framework of cells and helps them divide, move and maintain their shape. This dynamic and adaptive structure is composed of three main types of filaments, distinguishable by their size: actin filaments or microfilaments, microtubules and a group of polymers collectively known as intermediate filaments[31,35]. At present, IFs are the least characterized filaments of the cytoskeleton, and our current knowledge at the level of mature filaments is still far from complete, as the exact three-dimensional structure of the filaments, as well as the dynamic processes of filament maturation, are yet to be fully understood. This shortage of knowledge regarding the organization and dynamics of IFs, and in particular of GFAP, is attributed, at least in part, to the lack of chimeric versions of GFAP, making it difficult to visualize and study this protein *in vivo*. In fact, the attachment of protein tags directly to the N- or C-termini of GFAP cause a disruption of the filament network and increase the tendency of the protein to aggregate[84]. In this sense, our study aimed to create new molecular tools to study the behavior of GFAP in living cells.

In this work, we started by developing a new tool to study the behavior of mouse GFAP. EGFP-tagged mouse GFAP has been previously used to study GFAP function and dynamics[110]. This was the first time GFAP was successfully tagged, and it was thanks to the introduction of a flexible molecular linker between GFAP and EGFP, which enabled correct folding of GFAP and facilitated the integration of GFAP within the endogenous intermediate filament network of U251 glioma cells. However, biophysical and photophysical limitations of the green fluorescent proteins and its variants make them unusable in some super-resolution microscopy and in long live-cell experiments[104,105]. In order to study the architecture and behavior of GFAP at a nanoscopic level in living cells, we constructed a mouse-GFAP-HaloTag (mGFAP-HT) fused plasmid, keeping the molecular linker between GFAP and HaloTag. The HaloTag is an attractive alternative to fluorescent tags approach because it combines the genetic specificity of fluorescent proteins with the superior photophysics of organic dyes[106].

While studies using fluorescently tagged mouse GFAP have been previously reported, no studies have been published involving fluorescently tagged human GFAP. In this study, we also successfully developed the first tagged version of human GFAP, by inserting an EGFP tag inside the coding region of GFAP (hGFAP-EGFP). This protein tag was inserted by a randomized approach between amino acids 181 and 183 in the segment 1B of the conserved rod-domain of GFAP. Interestingly, this region contains very few mutations related to Alexander disease[61]. Our hGFAP-EGFP construct, like the mGFAP-HT construct, was able to successfully form a filamentous network when expressed in U251 cells. GFAP behavior is not universal and the ability of this protein to form filaments depends strongly on the cellular environment. Our results demonstrate that our hGFAP construct is more versatile that the mGFAP, as it was able to produce filaments in both human and rat cells, opposingly to the mGFAP construct, which only produced filaments when transfected into human cells. We also used our hGFAP-EGFP construct as a host vector for the generation of a hGFAP-BiFC system and a hGFAP-HT plasmid, but without success. Both constructs did not form any filamentous structures in living cells but instead formed small aggregates in the cytoplasm of the cells. We speculate that the introduction of these tags disrupts the normal folding of GFAP and increases the tendency of the protein to aggregate. We are currently considering the possibility to add linkers between the tags and the surrounding GFAP sequence.

Previous studies reported that Alexander disease mutations disturb *in vitro* filament assembly and network formation by GFAP[80,110]. The evidence that the mouse R236 or the human R239 mutations in GFAP interfere with filament assembly is further supported by the fact that a mutation homologous to

this, R249Q, has been found in the type-V intermediate filament lamin A/C[111]. This mutation affects the structure of nuclear lamin, and patients with this mutation develop autosomal dominant Emery-Dreifuss muscular dystrophy. Furthermore, structures that resemble Rosenthal fibers have been observed in myopathies caused by dominant mutations in the intermediate filament desmin[112]. Our results confirm these observations, as the majority of cells expressing mouse R236H or human R239C mutant GFAP do not display a typical filamentous network. While the human R239C mutant is mostly organized in inclusions, mouse R236H mutant GFAP formed a homogeneous pattern without apparent filament structures. This observation contrasts a previous study[110], where mutant R236H mouse GFAP-EGFP tagged predominantly formed aggregates. This difference could be due to the difference of tags, as the HaloTag might be inhibiting the formation of aggregates. Additionally, mutant GFAP does not behave the same in all cells[80], as in some cells mutant GFAP was able to incorporate into the endogenous GFAP network and form filamentous structures. Murine models of AxD[87,113] showed that overexpression (approximately 3-fold increase) of mutated GFAP is an important factor in its aggregation. However, we observed aggregate formation in our hGFAP-EGFP model without an obvious increase in GFAP levels. Accumulation of GFAP without an overall increase in its levels may represent an early stage of disease and suggests that mutations in GFAP are sufficient to induce aggregation.

Although some efforts have been made toward the discovery of drugs and compounds against AxD, the truth is that this disease remains uncurable. Recent findings, however, demonstrated a beneficial effect of the spice curcumin, in reducing GFAP accumulation[114]. To improve the effectiveness of curcumin, two synthetic derivatives of curcumin, J147[115] and CNB-001[116] were previously synthesized by Dr. Schubert's laboratory (The Salk Institute, CA, USA). Of the two, J147 is the best-studied curcumin derivative and has been proven effective in various rodent models of neurodegenerative disease and memory enhancement[117,118]. CNB-001 has been proven to have a neuroprotective activity in cell culture assays[116]. When we tested the neuroprotective activities of these two molecules in a cellular model of AxD, we observed that only CNB-001, and at a concentration of 10 μM, showed a slight but significant increase in filament formation and a decrease in GFAP accumulation. Our data support the hypothesis that CNB-001 does have a beneficial role in reducing GFAP accumulation and that CNB-001 is more efficient than J147, at least in our cellular model of AxD. As curcumin proved to be best efficient in a concentration range between 15-40 μM[114], further studies will need to be done using higher concentrations of J147 and CNB-001, to find out what is the most beneficial concentration of each compound. A recent report[119] showed that the neuroprotective properties of J147 came from its binding and partial inhibition of the activity of ATP synthase, which in turn causes an increase in intracellular calcium and activates the AMPK/mTOR pathway, which is involved in cell growth, proliferation, and survival. The cellular targets of CNB-001 are not known, but it is hypothesized that this drug might share some positive pharmacological traits with curcumin, such as its ability to stimulate innate neuroprotective pathways via the activation of phase 2 enzymes[116].

There is increasing evidence demonstrating that IFs are highly dynamic structures that are constantly rearranging in response to various stimuli. However, their dynamic properties remain unclear. In this study, we used single-molecule techniques to probe the motility of individual GFAP molecules in living cells. By labeling our mGFAP-HT construct with the fluorescent HaloTag ligand PA-JF549, we showed that the R236H AxD-related mutation has a strong effect on the dynamics of GFAP molecules. In fact, the mutation appears to increase the rate of diffusion of GFAP, which at first sight seems to contradict a previously proposed model[58,67] in which the effect of the mutations is to slow down the rate of polymer formation. We find two possible interpretations for our results. First, AxD-inducing mutations could increase the rate of filamentation that pushes the boundaries of the fibril dynamics to a breaking point, as the rate of removal of old monomers from the fiber does not occur at the same speed

as the entrance of new monomers in the fiber. This could create a "traffic jam" in the fiber, and favor the production of aggregates, collapse of filaments or aberrant interactions with close filaments or other proteins. Alternatively, our data showing faster diffusion could be interpreted as poorer formation of fibers, which could increase the number of free diffusing GFAP monomers. While it is clear that AxD mutations disrupt fiber formation, further analysis will be needed to ascertain the exact mechanism.

IFs are in constant communication with the other elements of the cytoskeleton, and very often their dynamics requires the participation of microtubules and actin filaments. Consistent with recent findings[14], depolymerization of actin microfilaments or microtubules resulted in a significant reduction of the diffusion of GFAP and an increase in the percentage of immobile/slow-diffusing molecules. Our findings demonstrate that actin depolymerization has a stronger effect in decreasing GFAP diffusion than microtubule depolymerization. This result, however, seems to disagree with the finding that actin depolymerization does not block the emergence of fast-moving IFs along microtubules[14], so we would expect that the diffusion of GFAP molecules would be slower when we depolymerize microtubules. This discrepancy may result from a partial depolymerization of microtubules, as we did not incubate the cells at 4ºC before adding Nocodazole, as some authors suggest[120].

Our dynamics data result from fitting the different trajectories to a 2-state kinetic model, where we assume the existence of two populations with different diffusion properties: one population with a very slow diffusion, that might represent GFAP molecules inside fibers, and another population of molecules not in fibers with a faster diffusion. This is, however, a simplification of the actual number of different GFAP populations that might exist in a cell. Some suggest that IFs can be found in at least three different forms: mature filaments, short filaments of different sizes and non-filamentous particles[120]. Our data fit very well to a 2-state model and this might be due to the fact that, with our imaging settings, we were unable to continuously track GFAP particles or small structures as they move too fast and quickly go out-of-focus. A way to image this fast-diffusion population is by increasing the laser power and faster imaging (reduce the exposure time); this will also increase the rate of PA-JF549 photobleaching and allow for a higher density of molecules to be tracked at the expense of shorter trajectory lengths. Another way to get more and longer tracks is by introducing three-dimensional imaging (Z-stacks), which would allow the tracking of molecules that quickly go out-of-focus. However, doing Z-stack acquisitions may decrease temporal resolution of particles that are always in the same plane. An alternative to collecting Z-stacks is encoding Z position in the shape of the image of a molecule by phase modulation, which can localize a molecule through ~5 μm at the expense of lower signal: noise and lower density during acquisition. We are currently studying these possibilities in order to make a more complete and accurate description of GFAP behavior.

In sum, in this thesis, we developed two novel and versatile systems for the study of GFAP behavior in living cells, and that can easily be applied for the study of other IFs. The development of new and more versatile molecular tools, however, continues to be indispensable to better understand the function, structure, and dynamics of GFAP in living cells, and to understand the mechanisms by which GFAP mutations cause Alexander disease and lead to astrocyte dysfunction.

6. Main Conclusions

In the present study, we successfully developed two novel systems to study the behavior of GFAP in normal and AxD-related conditions, a new and more versatile tool for the study of mouse GFAP by super-resolution microscopy or other advanced methods and the first tagged version of human GFAP. These tools allowed us to conclude that:

1. The ability of tagged GFAP to form filaments depends strongly on the cellular environment and the tags themselves;
2. Mouse R236H and human R239C AxD-causing mutations are deleterious to the assembly and network formation and alter the dynamic properties of the intermediate filament GFAP; and
3. GFAP dynamics and network maintenance are tightly associated to the dynamics of the other cytoskeleton proteins.

7. References

1. Wickstead B, Gull K (2011). The evolution of the cytoskeleton. J Cell Biol. 194: 513–525.
2. Fletcher DA, Mullins RD (2010). Cell mechanics and the cytoskeleton. Nature 485-492.
3. Hardin J, Bertoni G, Kleinsmith LJ, Becker WM (2012). Becker's world of the cell (8th ed.). Boston: Benjamin Cummings.
4. Pollat TD, Goldman RD (2017). Overview of the cytoskeleton from an evolutionary perspective. Cold Spring Harb Perspect Biol. 10: a030288.
5. Magin TM, Reichelt J, Hatzfeld M (2004). Emerging functions: diseases and animal models reshape our view of the cytoskeleton. Exp Cell Res. 301: 91–102.
6. Guzenko D, Chernyatina AA, Strelkov SV (2017). Crystallographic studies of intermediate filament proteins. Subcell. Biochem 82: 151–170.
7. Omary MB, Coulombe PA, McLean WH (2004). Intermediate filament proteins and their associated diseases. New Engl J Med. 351: 2087–2100.
8. Omary MB (2009). "IF-pathies": a broad spectrum of intermediate filament–associated diseases. J Clin Investig. 119: 1756–1762.
9. Parry DA, Strelkov SV, Burkhard P, Aebi U, Herrmann H (2007). Towards a molecular description of intermediate filament structure and assembly. Exp Cell Res. 313: 2204-2216.
10. Strelkov SV, Herrmann H, Aebi U (2003). Molecular architecture of intermediate filaments. BioEssays 25: 243–251.
11. Chernyatina AA, Guzenko D, Strelkov SV (2015). Intermediate filament structure: the bottom-up approach. Curr Opin Cell Biol. 32: 65–72.
12. Starger JM, Brown WE, Goldman AE, Goldman RD (1978). Biochemical and immunological analysis of rapidly purified 10-nm filaments from baby hamster kidney (BHK-21) cells. J Cell Biol. 78: 93–109.
13. Robert A, Hookway C, Gelfand VI (2016). Intermediate filament dynamics: what we can see now and why it matters. BioEssays 38: 232–243.
14. Leduc C, Etienne-Manneville S (2017). Regulation of microtubule-associated motors drives intermediate filament network polarization. J Cell Biol. 216: 1689–1703.
15. Dupin I, Etienne-Manneville S (2011). Nuclear positioning: mechanisms and functions. Int. J Biochem Cell Biol. 43: 1698–1707.
16. Dupin I, Sakamoto Y, Etienne-Manneville S (2011). Cytoplasmic intermediate filaments mediate actin-driven positioning of the nucleus. J Cell Sci. 124: 865–872.
17. Schwarz N, Leube RE (2016). Intermediate filaments as organizers of cellular space: how they affect mitochondrial structure and function. Cells 5: E30.
18. Marceau N, Schutte B, Gilbert S, Loranger A, Henfling ME, Broers JL, Mathew J, Ramaekers FC (2007). Dual roles of intermediate filaments in apoptosis. Exp Cell Res. 313: 2265–2281.
19. Eriksson JE, Opal P, Goldman RD (1992). Intermediate filament dynamics. Curr Opin Cell Biol. 4: 99–104.
20. Foisner R (1997). Dynamic organisation of intermediate filaments and associated proteins during the cell cycle. BioEssays 19: 297–305.
21. Cheng F, Eriksson JE (2017). Intermediate filaments and the regulation of cell motility during regeneration and wound healing. Cold Spring Harb. Perspect. Biol. 9: a022046.

22. Leduc C, Etienne-Manneville S (2015). Intermediate filaments in cell migration and invasion: the unusual suspects. Curr Opin Cell Biol. 32: 102–112.

23. Parpura V, Heneka MT, Montana V, Oliet SH, Schousboe A, Haydon PG, Stout RF Jr, Spray DC, Reichenbach A, Pannicke T *et al.* (2012). Glial cells in (patho)physiology. J Neurochem 121: 4- 27.

24. Eng LF, Vanderhaeghen JJ, Bignami A, Gerstl B (1971). An acidic protein isolated from fibrous astrocytes. Brain Res. 28: 351–354.

25. Eng LF, Ghirnikar RS, Lee YL (2000). Glial fibrillary acidic protein: GFAP-thirty-one years (1969-2000). Neurochem Res. 25: 1439–1451.

26. Schnitzerb J, Franke WW, Schachner M (1981). Immunocytochemical demonstration of vimentin in astrocytes and ependymal cells of developing and adult mouse nervous system. J Cell Biol. 90: 435-447.

27. Bovolenta P, Liem RK, Mason CA (1984). Development of cerebellar astroglia: transition in form and cytoskeletal content. Dev Bid. 102: 248-259.

28. Pixley SK, de Vellis J (1984). Transition between immature radial glia and mature astrocytes studied with a monoclonal antibody to vimentin. Brain Res. 317: 201-209.

29. Sofroniew MV, Vinters HV (2010). Astrocytes: biology and pathology. Acta Neuropathologica, 119(1): 7–35.

30. Bongcam-Rudloff E, Nister M, Betsholtz, C, Wang JL, Stenman G, Huebner K, Croce CM, Westermark B (1991). Human glial fibrillary acidic protein: complementary DNA cloning, chromosome localization, and messenger RNA expression in human glioma cell lines of various phenotypes. Cancer Res. 51: 1553–1560.

31. Middeldorp J, Hol EM (2011). GFAP in health and disease. Prog Neurobiol 93: 421–443.

32. Kamphuis W, Mamber C, Moeton M, Kooijman L, Sluijs JA, Jansen AH, Verveer M, de Groot LR, Smith VD, Rangarajan S, *et al.* (2012). GFAP isoforms in adult mouse brain with a focus on neurogenic astrocytes and reactive astrogliosis in mouse models of Alzheimer disease. Plos One. 7(8): e42823.

33. Eun K, Hwang SU, Jeon HM, Hyun SH, Kim H (2016). Comparative Analysis of Human, Mouse, and Pig Glial Fibrillary Acidic Protein Gene Structures. Anim Biotechnol. 27: 126–132.

34. Reeves SA, Helman LJ, Allison A, Israel MA (1989). Molecular cloning and primary structure of human glial fibrillary acidic protein. Proc Natl Acad. Sci. USA. 86: 5178–5182.

35. Etienne-Manneville S (2018). Cytoplasmic intermediate filaments in cell biology. Annu Rev Cell Dev Biol. 34: 1-28.

36. Kornreich M, Avinery R, Malka-Gibor E, Laser-Azogui A, Beck R (2015). Order and disorder in intermediate filament proteins. FEBS Lett. 589: 2464–2476.

37. Sihag RK, Inagaki M, Yamaguchi T, Shea TB, Pant HC (2007). Role of phosphorylation on the structural dynamics and function of types III and IV intermediate filaments. Exp Cell Res. 313: 2098–2109.

38. Inagaki M, Gonda Y, Nishizawa K, Kitamura S, Sato C, Ando S, Tanabe K, Kikuchi K, Tsuiki S, Nishi Y (1990). Phosphorylation sites linked to glial filament disassembly in vitro locate in a non-alpha-helical head domain. J Biol Chem. 265: 4722–4729.

39. Inagaki M, Matsuoka Y, Tsujimura K, Ando S, Tokui T, Takahashi T, Inagaki N (1996). Dynamic property of intermediate filaments: regulation by phosphorylation. BioEssays 18: 481-487.

40. Nicholas AP, Sambandam T, Echols JD, Tourtellotte WW (2004). Increased citrullinated glial fibrillary acidic protein in secondary progressive multiple sclerosis. J Comp Neurol. 473: 128–136.

41. Moeton M, Kanski R, Stassen OM, Sluijs JA, Geerts D, van Tijn P, Wiche G, van Strien ME, Hol EM (2014). Silencing GFAP isoforms in astrocytoma cells disturbs laminin-dependent motility and cell adhesion. FASEB J 28: 2942–2954.

42. Guichet PO, Guelfi S, Ripoll C, Teigell M, Sabourin JC, Bauchet L, Rigau V, Rothhut B, Hugnot JP (2016). Asymmetric distribution of GFAP in glioma multipotent cells. PLoS One 11: e0151274.

43. Sekimata M, Tsujimura K, Tanaka J, Takeuchi Y, Inagaki N, Inagaki M (1996). Detection of protein kinase activity specifically activated at metaphase-anaphase transition. J Cell Biol 132: 635–641.

44. Potokar M, Stenovec M, Gabrijel M, Li L, Kreft M, Grilc S, Penky M, Zorec R (2010). Intermediate filaments attenuate stimulation-dependent mobility of endosomes/lysosomes in astrocytes. Glia 58: 1208-1219.

45. Potokar M, Vardjan N, Stenovec M, Gabrijel M, Trkov S, Jorgacevski J, Kreft M, Zorec R (2013). Astrocytic vesicle mobility in health and disease. Int J Mol Sci 14: 11238–11258.

46. Hughes EG, Maguire JL, McMinn MT, Scholz RE, Sutherland ML (2004). Loss of glial fibrillary acidic protein results in decreased glutamate transport and inhibition of PKA-induced EAAT2 cell surface trafficking. Brain Res Mol Brain Res 124: 114–123.

47. Sullivan SM, Lee A, Bjorkman ST, Miller SM, Sullivan RK, Poronnik P, Colditz PB, Pow DV (2007). Cytoskeletal anchoring of GLAST determines susceptibility to brain damage: an identified role for GFAP. J Biol Chem 282: 29414–29423.

48. Pekny M. (2001). Astrocytic intermediate filaments: lessons from GFAP and vimentin knockout mice. Prog Brain Res 132: 23–30.

49. Gomi H, Yokoyama T, Fujimoto K, Ikeda T, Katoh A, Itoh T, Itohara S (1995). Mice devoid of the glial fibrillary acidic protein develop normally and are susceptible to scrapie prions. Neuron 14: 29-41.

50. McCall MA, Gregg RG, Behringer RR, Brenner M, Delaney CL, Galbreath EJ, Zhang CL, Pearce RA, Chiu SY, Messing A (1996). Targeted deletion in astrocyte intermediate filament (Gfap) alters neuronal physiology. Proc Natl Acad Sci USA 93: 6361-6366.

51. Pekny M, Leveen P, Pekna M, Eliasson C, Berthold CH, Westermark B, Betsholtz C (1995). Mice lacking glial fibrillary acidic protein display astrocytes devoid of intermediate filaments but develop and reproduce normally. EMBO J 14: 1590-1598.

52. Nawashiro H, Messing A, Azzam N, Brenner M (1998). Mice lacking GFAP are hypersensitive to traumatic cerebrospinal injury. Neuroreport 9: 1691-1696.

53. Triolo, D, Dina G, Lorenzetti I, Malagutti M, Morana P, del Carro U, Comi G, Messing A, Quattrini A, Previtali SC (2006). Loss of glial fibrillary acidic protein (GFAP) impairs Schwann cell proliferation and delays nerve regeneration after damage. Journal of cell science, 119: 3981–3993.

54. Seifert G, Schilling K, Steinhauser C (2006). Astrocyte dysfunction in neurological disorders: a molecular perspective. Nat Rev Neurosci 7: 194-206.

55. Burda JE, Sofroniew MV (2014). Reactive gliosis and the multicellular response to CNS damage and disease. Neuron 81: 229-248.

56. Hostenbach S, Cambron M, D'haeseleer M, Kooijman R, De KJ (2014). Astrocyte loss and astrogliosis in neuroinflammatory disorders. Neurosci Lett 565: 39-41.

57. Sriram K, Benkovic SA, Hebert MA, Miller DB, O'Callaghan JP (2004). Induction of gp130-related cytokines and activation of JAK2/ STAT3 pathway in astrocytes precedes up-regulation of glial fibrillary acidic protein in the 1-methyl-4-phenyl-1,2,3, 6-tetrahydropyridine model of neurodegeneration: key signaling pathway for astrogliosis *in vivo*? J Biol Chem 279: 19936-19947.

58. Messing A, Brenner M, Feany MB, Nedergaard M, Goldman JE (2012). Alexander disease. J Neurosci. 32: 5017–5023.

59. Alexander WS (1949). Progressive fibrinoid degeneration of fibrillary astrocytes associated with mental retardation in a hydrocephalic infant. Brain 72: 373–381.

60. Yoshida T, Sasaki M, Yoshida M, Namekawa M, Okamoto Y, Tsujino S, Sasayama H, Mizuta I, Nakagawa M (2011). Nationwide survey of Alexander disease in Japan and proposed new guidelines for diagnosis. J Neurol. 258: 1998 –2008.

61. Messing A. (2018). Alexander disease. Handbook of Clinical Neurology. 148: 693-700.

62. Russo Jr LS, Aron A, Anderson PJ (1976). Alexander's disease: a report and reappraisal. Neurology 26: 607–614.

63. Prust M, Wang J, Morizono H, Messing A, Brenner M, Gordon E, Hartka T, Sokohl A, Schiffmann R, Gordish-Dressman H *et al.* (2011). GFAP mutations, age of onset, and clinical sub-types in Alexander disease. Neurology 77: 1287–1294.

64. Brenner M, Johnson AB, Boespflug-Tanguy O, Rodriguez D, Goldman JE, Messing A (2001). Mutations in GFAP, encoding glial fibrillary acidic protein, are associated with Alexander disease. Nat Genet 27: 117–120.

65. Brenner M, Goldman JE, Quinlan RA, Messing A (2009). Alexander disease: a genetic disorder of astrocytes. In: Astrocytes in (patho)physiology of the nervous system (Parpura V, Haydon PG, eds), pp 591–648. New York: Springer.

66. Li R, Johnson AB, Salomons G, Goldman JE, Naidu S, Quinlan R, Cree B, Ruyle SZ, Banwell B, D'Hooghe M *et al*. (2005). Glial fibrillary acidic protein mutations in infantile,juvenile, and adult forms of Alexander disease. Ann Neurol. 57: 310–326.

67. Li R, Messing A, Goldman JE, Brenner M (2002). GFAP mutations in Alexander disease. Int J Devl. Neuroscience. 20: 259–268.

68. Johnson AB (2002). Alexander disease: a review and the gene. Int J Devl Neuroscience 20: 391–394.

69. Tomokane N, Iwaki T, Tateishi J, Iwaki A, Goldman JE (1991). Rosenthal fibers share epitopes with alpha B-crystallin, glial fibrillary acidic protein, and ubiquitin, but not with vimentin. Immunoelectron microscopy with colloidal gold. Am J Pathol. 138: 875–885.

70. Der Perng M, Su M, Wen SF, Li R, Gibbon T, Prescott AR, Brenner M, Quinlan RA (2006). The Alexander disease-causing glial fibrillary acidic protein mutant, R416W, accumulates into Rosenthal fibers by a pathway that involves filament aggregation and the association of alpha B-crystallin and HSP27. Am J Hum Genet. 79: 197–213.

71. Heaven MR, Flint D, Randall SM, Sosunov AA, Wilson L, Barnes S, Goldman JE, Muddiman DC, Brenner M (2016). Composition of Rosenthal fibers, the protein aggregate hallmark of Alexander disease. J Proteome Res. 115: 2265–2282.

72. Head MW, Corbin E, Goldman JE (1994). Coordinate and independent regulation of alpha B-crystallin and hsp27 expression in response to physiological stress. J Cell Physiol 159: 41–50.

73. Perng MD, Cairns L, van den IP, Prescott A, Hutcheson AM, Quinlan R (1999). Intermediate filament interactions can be altered by HSP27 and alphaB-crystallin. J Cell Sci 112: 2099–2112.

74. Mehlen P, Preville X, Chareyron P, Briolay J, Klemenz R, Arrigo AP (1995). Constitutive expression of human hsp27, Drosophila hsp27, or human alpha B-crystallin confers resistance to TNF- and oxidative stress-induced cytotoxicity in stably transfected murine L929 fibroblasts. J Immunol 154: 363–374.

75. Sosunov AA, McKhann GM, Goldman JE (2017). The origin of Rosenthal fibers and their contributions to astrocyte pathology in Alexander disease. Acta Neuropathol Commun. 5: 27.

76. Sun DA, Yu H, Spooner J, Tatsas AD, Davis T, Abel TW, Kao C, Konrad PE (2008). Postmortem analysis following 71 months of deep brain stimulation of the subthalamic nucleus for Parkinson disease. J Neurosurg. 109: 325 – 329.

77. Louis DN, Ohgaki H, Wiestler OD, Cavenee WK (eds) (2016). WHO Classification of Tumours of the Central Nervous System, 4th edn. Lyon, France: IARC.

78. Sosunov A, Olabarria M, Goldman JE (2018). Alexander disease: an astrocytopathy that produces a leukodystrophy. Brain Pathology 28: 388–398.

79. Messing A, Head MW, Galles K, Galbreath EJ, Goldman JE, Brenner M (1998). Fatal encephalopathy with astrocyte inclusions in GFAP transgenic mice. Am J Path. 152: 391–398.

80. Hsiao VC, Tian R, Long H, Der Perng M, Brenner M, Quinlan RA, Goldman JE (2005). Alexander-disease mutation of GFAP causes filament disorganization and decreased solubility of GFAP. J Cell Sci. 118: 2057–2065.

81. Chen YS, Lim SC, Chen MH, Quinlan RA, Perng MD (2011). Alexander disease causing mutations in the C-terminal domain of GFAP are deleterious both to assembly and network formation with the potential to both activate caspase 3 and decrease cell viability. Exp Cell Res 317: 2252–2266.

82. Tang G, Perng MD, Wilk S, Quinlan R, Goldman JE (2010). Oligomers of mutant glial fibrillary acidic protein (GFAP) inhibit the proteasome system in Alexander disease astrocytes, and the small heat shock protein, αB-crystallin, reverses the inhibition. J Biol Chem 285: 10527–10537.

83. Cho W, Messing A (2009) Properties of astrocytes cultured from GFAP over-expressing and GFAP mutant mice. Exp Cell Res 315: 1260 –1272.

84. Tang G, Xu Z, Goldman JE (2006) Synergistic effects of the SAPK/JNK and the proteasome pathway on glial fibrillary acidic protein (GFAP) accumulation in Alexander disease. J Biol Chem 281: 38634–38643.

85. Tang G, Yue Z, Talloczy Z, Hagemann T, Cho W, Messing A, Sulzer DL, Goldman JE (2008). Autophagy induced by Alexander disease-mutant GFAP accumulation is regulated by p38/MAPK and mTOR signalling pathways. Hum Mol Genet 17: 1540 –1555.

86. Hagemann TL, Gaeta SA, Smith MA, Johnson DA, Johnson JA, Messing A (2005). Gene expression analysis in mice with elevated glial fibrillary acidic protein and Rosenthal fibers reveals a stress response followed by glial activation and neuronal dysfunction. Hum Mol Genet 14: 2443–2458.

87. Hagemann TL, Connor JX, Messing A (2006). Alexander disease-associated glial fibrillary acidic protein mutations in mice induce Rosenthal fiber formation and a white matter stress response. J Neurosci 26: 11162–11173.

88. Jones JR, Kong L, Hanna MGIV, Hoffman B, Krencik R, Bradley R, Hagemann T, Choi J, Doers M, Dubovis M, *et al.* (2018). Mutation in GFAP disrupt the distribution and function of organelle in human astrocytes. Cell Report 25: 947–958.

89. Tian R, Wu X, Hagemann TL, Sosunov AA, Messing A, McKhann GM, Goldman JE (2010). Alexander disease mutant glial fibrillary acidic protein compromises glutamate transport in astrocytes. J Neuropathol Exp Neurol. 69: 335–345.

90. Olabarria M, Putilina M, Riemer EC, Goldman JE (2015). Astrocyte pathology in Alexander disease causes a marked inflammatory environment. Acta Neuropathol 130: 469–486.

91. Messing A, LaPash Daniels CM, Hagemann TL (2010) Strategies for Treatment in Alexander Disease. Neurotherapeutics 7: 507–515.

92. Cho W, Brenner M, Peters N, Messing A (2010). Drug screening to identify suppressors of GFAP expression. Human Molecular Genetics 19: 3169-3178.

93. Rothstein JD, Patel S, Regan MR, Haenggeli C, Huang YH, Bergles DE, Jin L, Dykes Hoberg M, Vidensky S, Chung DS, Toan SV, Bruijn LI, Su ZZ, Gupta P, Fisher PB (2005) b-Lactam antibiotics offer neuroprotection by increasing glutamate transporter expression. Nature 433: 73–77.

94. Bachetti T, Di Zanni E, Balbi P, Bocca P, Prigione I, Deiana GA, Rezzani A, Ceccherini I, Sechi G (2010). In vitro treatments with ceftriaxone promote elimination of mutant glial fibrillary acidic protein and transcription down-regulation. Exp. Cell Res. 316: 2152–2165.

95. Sechi G, Matta M, Deiana GA, Balbi P, Bachettu T, Di Zanni E, Ceccherini I, Serra A (2010). Ceftriaxone has a therapeutic role in Alexander disease. Prog Neuropsychopharmacol Biol Psychiatry 34: 416 –417.

96. Vargas MR, Johnson DA, Sirkis DW, Messing A, Johnson JA (2008). Nrf2 activation in astrocytes protects against neurodegeneration in mouse models of familial amyotrophic lateral sclerosis. J Neurosci 25: 13574 - 13581.

97. Chen PC, Vargas MR, Pani AK, Smeyne RJ, Johnson DA, Kan YW, Johnson JA (2009). Nrf2-mediated neuroprotection in the MPTP mouse model of Parkinson's disease: critical role for the astrocyte. Proc Natl Acad Sci USA 106: 2933– 2938.

98. Hagemann TL, Boelens WC, Wawrousek EF, Messing A (2009). Suppression of GFAP toxicity by αB-crystallin in mouse models of Alexander disease. Hum Mol Genet 18: 1190–1199.

99. Tinevez JY, Perry N, Schindelin J, Hoopes GM, Reynolds GD, Laplatine E, Bednarek SY, Shorte SL, Eliceiri KW (2016). TrackMate: An open and extensible platform for single-particle tracking. Methods 115: 80-90.

100. Hansen AS, Woringer M, Grimm JB, Lavis LD, Tjian R, Darzacq X. (2018). Robust model-based analysis of single-particle tracking experiments with Spot-On. eLife 7: e333125.

101. Laine RF, Tosheva KL, Gustafsson N, Gray RDM, Almada P, Albrecht D, Risa GT, Hurtig F, Lindås AC, Baum B et al. (2019). NanoJ: a high-performance open-source super-resolution microscopy toolbox. J Phys D Appl Phys. 52

102. Tsien RY (1998). The green fluorescent protein. Annu Rev Biochem. 67: 509–544.

103. Uno SN, Tiwari DK, Kamiya M, Arai Y, Nagai T, Urano Y (2015). A guide to use photocontrollable fluorescent proteins and synthetic smart fluorophores for nanoscopy. Microscopy (Oxf.) 64: 263–277.

104. Dempsey GT, Vaughan JC, Chen KH, Bates M, Zhuang XW (2011). Evaluation of fluorophores for optimal performance in localization based super-resolution imaging. Nat. Methods 8: 1027–1035.

105. Fernandez-Suarez M, Ting AY (2008). Fluorescent probes for super resolution imaging in living cells. Nat. Rev. Mol. Cell Biol. 9: 929–943.

106. Los GV, Encell LP, McDougall MG, Hartzell DD, Karassina N, Zimprich C, Wood MG, Learish R, Ohane RF, Urh M *et al.* (2008). HaloTag: a novel protein labeling technology for cell imaging and protein analysis. ACS Chem. Biol. 3: 373–382.

107. Lord SJ, Lee H-LD, Moerner WE (2010). Single-molecule Spectroscopy and imaging of Biomolecules in living cells. Analytical Chemistry 82: 2192–2203.

108. Sheridan DL, Berlot CH, Robert A, Inglis FM, Jakobsdottir KB, Howe JR, Hughes TE (2002). A new way to rapidly create functional, fluorescent fusion proteins: random insertion of GFP with an in vitro transposition reaction. BMC Neurosci. 3: 7.

109. Kerppola TK (2006). Complementary methods for studies of protein interactions in living cells. Nat. Methods 3: 969–971.

110. Mignot C, Delarasse C, Escaich S, Della Gaspera B, Noé E, Colucci-Guyon E, Babinet C, Pekny M, Vicart P, Boespflug-Tanguy O *et al.* (2007). Dynamics of mutated GFAP aggregates revealed by real-time imaging of an astrocyte model of Alexander disease. Exp Cell Res. 313: 2766-2779.

111. Raffaele Di Barletta M, Ricci E, Galluzzi G, Tonali P, Mora M, Morandi L, Romorini A, Voit T, Orstavik KH, Merlini L, *et al.* (2000). Different mutations in the LMNA gene cause autosomal dominant and autosomal recessive Emery-Dreifuss muscular dystrophy. Am J Hum Genet 66: 1407-1412.

112. Dalakas MC, Park KY, Semino-Mora C, Lee HS, Sivakumar K, Goldfarb LG (2000). Desmin myopathy, a skeletal myopathy with cardiomyopathy caused by mutations in the desmin gene. N Engl J Med 342: 770–780.

113. Tanaka KF, Takebayashi H, Yamazaki Y, Ono K, Naruse M, Iwasato T, Itohara S, Kato H, Ikenaka K (2007). Murine model of Alexander disease: analysis of GFAP aggregate formation and its pathological significance. Glia 55: 617–631.

114. Bachetti T, Di Zanni E, Balbi P, Ravazzolo R, Sechi G, Ceccherini I (2012). Beneficial effects of curcumin on GFAP filament organization and down-regulation of GFAP expression in an in vitro model of Alexander disease. Exp Cell Res. 318: 1844–1854.

115. Chen Q, Prior M, Dargusch R, Roberts A, Riek R, Eichmann C, Chiruta C, Akaishi T, Abe K, Maher P *et al.* (2011). A novel neurotrophic drug for cognitive enhancement and Alzheimer's disease. PLoS ONE 6: e27865.

116. Liu Y, Dargusch R, Maher P, Schubert D (2008). A broadly neuroprotective derivative of curcumin. J Neurochem. 105: 1336-1345.

117. Prior M, Goldberg J, Chiruta C, Farrokhi C, Kopynets M, Roberts AJ, Schubert D (2016). Selecting for neurogenic potential as an alternative for Alzheimer's disease drug discovery. Alzheimers Dement. 12: 678–686.

118. Currais A, Goldberg J, Farrokhi C, Chang M, Prior M, Dargusch R, Daugherty D, Armando A, Quehenberger O, Maher P *et al.* (2015). A comprehensive multiomics approach toward understanding the relationship between aging and dementia. Aging 7: 937–955.

119. Goldberg J, Currais A, Prior M, Fischer W, Chiruta C, Ratliff E, Daugherty D, Dargusch R, Finley K, Esparza-Moltó PB *et al.* (2018). The mitochondrial ATP synthase is a shared drug target for aging and dementia. Aging Cell 17: 1–13.

120. Robert A, Rossow MJ, Hookway C, Adam SA, Gelfand VI (2015). Vimentin filament precursors exchange subunits in an ATP-dependent manner. Proc Natl Acad Sci USA 112: E3505–E3514.